NO VTT-R-02391-09 | 30.3.2009

LAINE

Summary report of the project: Nonlinear wave loads of ships

Authors: Timo Kukkanen

Confidentiality: Public

Report's title	
Summary report of the project: Nonlinear wave loads of ships	
Customer, contact person, address TEKES 1604/31/06	Order reference 40334/06
Project name Laivojen epälineaariset aaltokuormat Nonlinear wave loads of ships	Project number/Short name 8697 / LAINE
Author(s) Timo Kukkanen	Pages 44/
Keywords Seakeeping, wave loads, model tests, numerical methods	Report identification code VTT-R-02391-09

Summary

Hydrodynamic responses in waves and especially nonlinearities in the hull girder loads were investigated in the project LAINE. One of the aims was to get insight of design wave loads for novel ship types and to obtain reliable numerical method for nonlinear ship-wave interaction problems. The project consisted of experimental investigations and theoretical background of nonlinear effects was studied and numerical methods was developed and applied.

The calculation method was based on time domain representation of the Green function. Exact body boundary condition was applied on the body surface. The most time consuming part was the solution of the Green function. The Green function was solved beforehand using finite element presentations and during the simulation the interpolation was performed applying finite element shape functions.

Validation and verification were given for the hemisphere and the Wigley hull form. For the hemisphere the calculated added mass and damping coefficients correlated well with analytical solution. For Wigley hull the responses were well predicted comparing to the model test results.

Model tests were carried out for Seatech-D ship model to measure ship motions and hull girder loads. The calculations gave good predictions for the nonlinear wave induced responses comparing to the model test results. The hull girder loads deviated somewhat from the model test results at zero speed. One reason was the flat stern bottom close to water line. The change in geometry due to the relative motions is challenging in the calculations and the effects due to rapid changes in hull geometry at flat stern bottom should be further studied.

Confidentiality	Public

Espoo 30.3.2009

Signatures	Signatures	Signatures
Written by Timo Kukkanen Senior Research Scientist	Reviewed by Heikki Helasharju Research Scientist	Accepted by Seppo Kivimaa Technology Manager

VTT's contact address
VTT, P.O.Box 1000, 02044 VTT

Distribution (customer and VTT)
Customers, 5 copies
VTT, 1 copy

Preface

Common practice in ship design is to determine the wave loads by applying rules and standards. The design rules and requirements are important to obtain international quality standards and design basis for ships. For example, Unified Requirements and Common Structural Rules for Bulkers and Tankers have been developed within International Association of Classification Societies (IACS) to improve safety of bulkers and tankers and to rationalise rules and requirements between different classification societies. In addition, Goal Based Standards for ship construction are under construction in International Maritime Organization (IMO). It is possible also that the role of ship owners in design process is coming more important in the future. Ship owners can set additional requirements and the designer has to prove that the ship will fulfil the requirements already in early design phase.

However, general standards and rules can be sometimes difficult to apply for unconventional ships. For example, size of the ships is increasing and new structural designs have been introduced. For complex structures and designs direct calculation procedures are necessary. The direct calculation of the wave loads in the structural analysis is nowadays a common practice in the offshore industry. However, the direct calculation procedures, especially the calculation of the wave loads, are seldom applied in the shipbuilding industry. One reason is the rather large uncertainties in the wave load predictions for ships as well as lack of experience. In addition the theoretical background of the calculation methods are not necessarily sufficient to get reliable predictions. For example, the forward speed of the ship is not properly taken into account in the methods or the methods are based on linear theory so that extreme load predictions of the nonlinear responses are not possible. Furthermore uncertainties exit also in all assumptions involved in stochastic methods and prediction procedures including environmental and operational conditions. Sometimes these are difficult to determine accurately in advance and hence assumptions need to be made to estimate life time conditions that have influence on fatigue and ultimate strength. Fatigue strength predictions can vary significantly depending on applied approaches and how different conditions are taken into account.

Project “Laine - A numerical and experimental study of nonlinear wave loads on ships”, was started at VTT in Merike - Technology Program in the autumn 2006. Participants of the project were Finnish Funding Agency for Technology and Innovation (TEKES), VTT, Aker Yards, Technip Offshore Finland, Finnish Navy and SWECO Marine. The aim of the project was to get insight of design wave loads for novel ship types and to develop calculation methods and procedures to estimate wave loads. The project consisted of numerical and experimental investigations. Theoretical background of nonlinear effects was studied and numerical methods was developed and applied during the project.

Espoo 30.3.2009, Authors

Contents

1 Introduction

1.1 Background

Elements in the load and strength analysis of marine structures are presented in Figure 1.1. One of the starting point for the structural design and analysis of the ships and marine structures is to define environmental and operational conditions. For ultimate strength analyses, extreme environmental conditions have to be defined in order to obtain the design loads for structural analyses. Typically the extreme condition is the most severe sea state in the ship's lifetime that induces the largest stresses in structural details. Because different wave conditions or different types of loads might induce large stresses, several different conditions have to be considered. In a fatigue analysis, the whole operational profile of a ship is needed to obtain all the stress cycles that the ship will encounter during her service life. This means that all of the different loading and operational conditions in the ship's lifetime have to be considered. In addition, because the random nature of the ocean waves, probabilistic methods have to be applied in the analyses. To obtain predictions in reasonable time, the calculations are usually carried out in the frequency domain by linear methods (Kukkanen and Mikkola, 2004). Responses are linear with respect to excitation, if a change in the magnitude of excitation induces the same magnitude change for responses. However, in high waves the linearity assumption of wave loads with respect to wave height is not usually valid. For example, the sagging moment is clearly larger than the hogging moment for ships in a heavy sea. If the responses are strongly nonlinear the determination of loads are usually carried out in time domain.

Environmental conditions are typically defined by the waves, winds and currents. Depending on the operation of the ship or marine structures some other factors can be equally important or even more important, e.g. ice or water depth. In here the main emphasis will be focused on waves. The waves and their occurrence probabilities are normally given in wave scatter diagrams for different sea areas, for example, Global Wave Statistics (GWS, 1986). For the extreme wave loads of the ships, the International Association of Classification Societies (IACS, 2001) gives recommendations to use the wave data of the North Atlantic sea area. In rules this sea area is usually defined as the worst sea area and it is intended to use to design ships for unrestricted service. Typically the North-Atlantic data is use for ultimate strength analyses but fatigue strength is predicted applying more realistic sea areas. If the route or operating area of the ship or marine structure is known in design phase site specific scatter diagram can be utilised. However, this can be difficult if the route of ship is not known beforehand. Det Norske Veritas (DNV, 2005) has produced a scatter diagram that is combination of different sea areas where the ships typically sail world wide.

The main operational conditions for ships are the speed and heading with respect to waves. The operational profile can vary considerably between different ship types. Depending of the ship type other operational conditions should be also taken into account, for example, loading conditions and time spent in harbour. Furthermore, voluntary speed reduction or possible restrictions in speed or heading in high waves should be considered in order to define extreme waves where the ship can safely operate.

The return period is defined as a event that is being exceeded on the average once every n-year. Usually the return period is used to define so called n-year wave. Thus the n-year wave is a wave that is being exceeded once every n-year. The return period is not necessary the same as the service time of the ship or marine structures. For example, in offshore structures the 100-year wave is one of the typical design condition.

In ship structural design the wave load and response predictions are often defined at the probability level of 10^{-8}. This corresponds of an occurrence that is expected to encounter once in 20-25 years. In the IACS recommendations (IACS, 2001) a return period of at least 20 years, corresponding to about 10^{-8} probability of exceedance per cycle is recommended to use for design wave bending moments. It can be noticed that the IACS recommendations relate the return period of 20 years and probability level 10^{-8}. Thus, for ships the return period corresponds to the service time of the ship. However, for the offshore structures the return period is used for environmental conditions that occur seldom and hence including higher safety margin against loads. This is justified because ships can avoid the heavy weather easily changing the route but offshore structures should be able to withstand all possible weather conditions that might occur in the sea area during the service time.

The uncertainties in wave load prediction can be taken into account using safety factors, for example using extreme values with additional risk parameter instead of using the conventional most probable extreme value. In addition, appropriate safety and usage factors are used in structural designs and the safety margin can be higher for critical structures. In ultimate strength analyses, part of the structures can be designed above the elastic limits to allow some extent of plastic deformations. It is important also to define the strength and fatigue criteria together with the safety factors in order to take into account all possible uncertainties in loads and structural designs. Because different safety factors can be used in different stages in structural design and analyses it is important to realise the overall margin of safety from environmental conditions to the strength criteria of structures. In addition, appropriate strength criteria and safety levels, i.e. safety margins or factor of safety, should be defined in particularly if first principle methods are be applied.

Wave loads are given for ships in rules of classification societies that are generally used in ship design. In present rules the rule loads and structural responses can be determined separately, e.g. external pressures and wave bending moments can be first determined and then use to determine structural scantlings. In principle, the rule loads can be compared to the loads calculated by direct methods. However, the rule requirements for loads and structural responses are still related to each other to fulfil the strength criteria. The rule loads and directly calculated loads can be compared but the final structural scantlings can depend on the used strength criteria.

Direct calculations of wave loads in structural analyses are generally based on linear theories but recently several different approaches have been developed to take into account nonlinearities in wave load predictions. Summary of different methods in seakeeping computations are given by Beck and Reed (2000). Usually the linear frequency domain methods give reliable results at zero speed. However, significant differences can exist between different nonlinear methods (Guedes Soares *et al*, 2000).

Environmental conditions

H_s (m) \ T_z (s)	4.5	5.5	6.5	7.5	8.5	9.5	10.5	11.5	12.5	13.5
11.5						1				
10.5					1	1	1			
9.5					1	2	2	1	1	
8.5				1	2	3	3	2	1	
7.5				1	4	6	5	3	1	
6.5			1	3	9	12	9	4	2	1
5.5			1	9	20	22	15	6	2	1
4.5			4	21	40	37	21	8	2	
3.5		1	12	45	67	50	22	7	2	
2.5		3	28	75	80	45	15	4	1	
1.5		9	48	73	48	17	4	1		
0.5	2	11	20	13	4	1				

Operational conditions

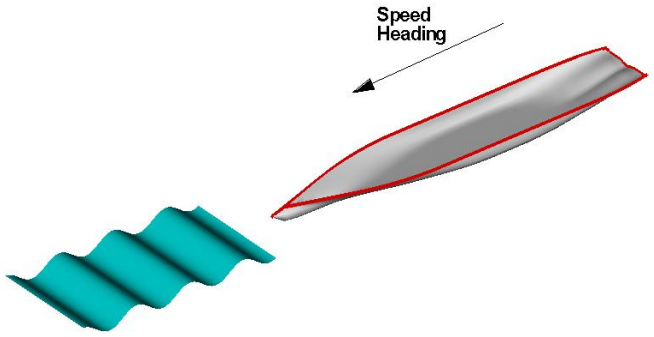

Responses in waves

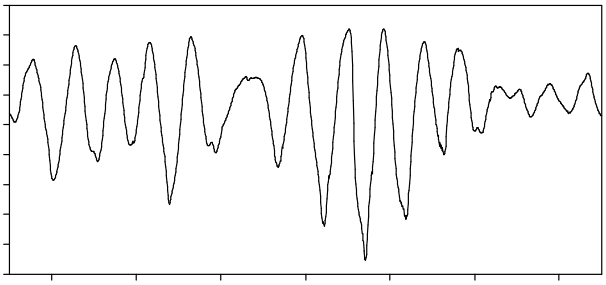

Extreme load and strength predictions

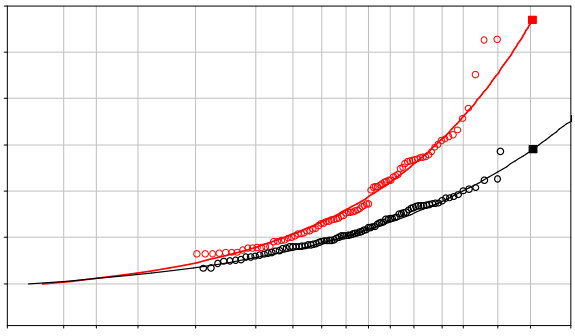

Fatigue strength predictions

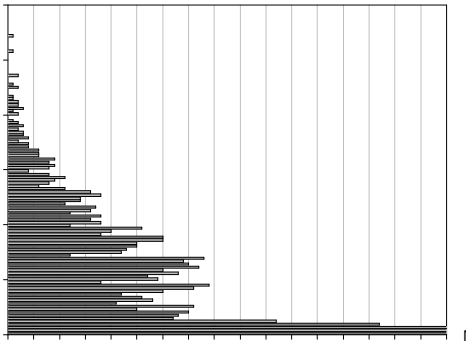

Figure 1.1. Elements in load and strength analyses of marine structures.

1.2 Objectives and scope

For ship type structures, an important wave induced response is the vertical wave bending moment that induces global hull girder stresses. If the hull girder has compression on deck it is called sagging condition and hogging if compression on bottom. The sagging bending moment occur if wave crests are at the bow and stern and hogging if wave crest is amidships. Typical example of time history in model tests for vertical bending moment amidships is shown in Figure 1.2 together with the calculation result based on the linear theory. The linear theories can not predict the differences between sagging and hogging moments. In the model test results higher order harmonic components are clearly visible and the time histories are not sinusoidal. The first harmonic component without the mean shift can be obtained only from the linear frequency domain wave load calculation methods. The linear methods can not take into account the body geometry above the mean water level especially the hull form changes at the bow and stern. In addition, the forward speed of the ship change the steady pressure and wave profile around the hull.

This project was focused on the hydrodynamic responses in waves and the emphasis was in the investigations on the nonlinear wave loads. Studies were concentrated on the nonlinear effects in the vertical bending moment. One of the aims of the present project was to get insight of design wave loads for novel ship types. Goal was to obtain reliable numerical method for nonlinear ship-wave interaction problems. In particular so that the calculated pressure loads acting on the hull surface can be used in the finite element analysis. The hydrodynamic pressures and the global finite element model of the ship hull is illustrated in Figure 1.3. In addition, statistical predictions were also studied in order to estimate the extreme loads in random waves for the ultimate strength analyses. Fatigue loading can be estimated from the time history results of the responses using a standard rainflow counting algorithm.

The project consisted of numerical and experimental investigations. Model test was carried out to get insight into the important factors of nonlinear effects and to obtain validation data for the numerical simulations. Theoretical background of nonlinear effects was studied and numerical methods was developed and applied during the project. In addition, approaches to predict extreme loads for structural analyses were examined.

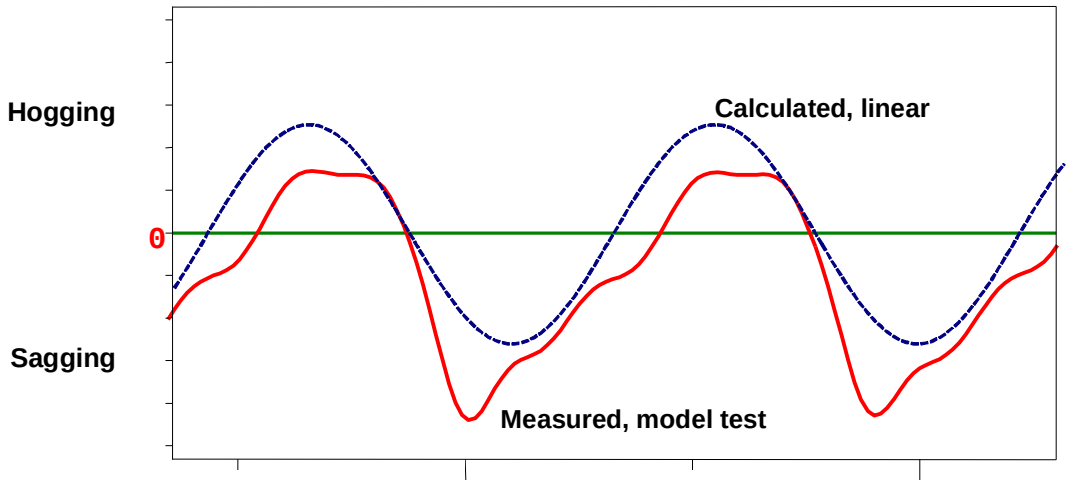

Figure 1.2. Typical example of time histories in model tests for vertical bending moment amidships and the linear calculation result.

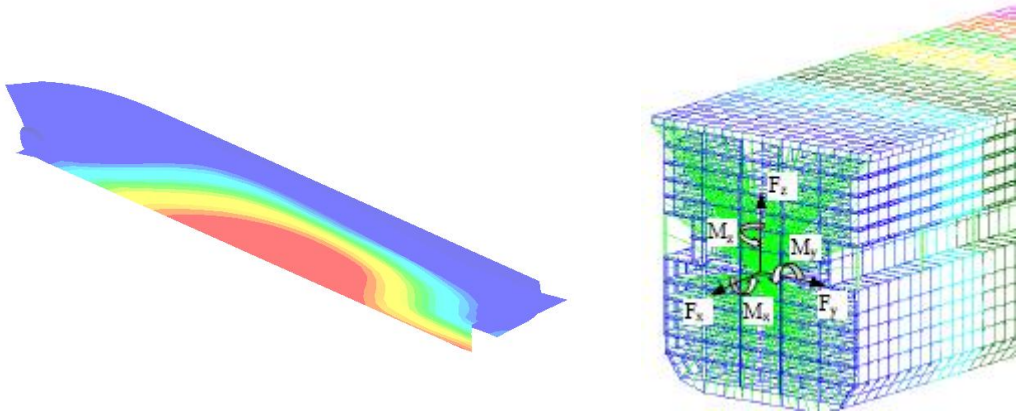

Figure 1.3. Pressure acting on the hull surface in waves and a global finite element model of a ship (Mäkinen, 2005).

2 Calculation method

2.1 General

A brief description is given here for the theoretical background of the boundary value problem of the moving body in water waves to give insight of the simplifications and their possible effects on the wave load predictions. Detailed derivation of the boundary value problem can be found, for example, from Newman (1978). Summary of different methods in seakeeping computations are given by Beck and Reed (2000).

It is assumed that the fluid is irrotational, incompressible and inviscid and hence the potential theory can be used to solve the flow around the body. The velocity potential has to fulfil the Laplace equations in the whole fluid domain and the boundary conditions at the free surface, bottom of the sea and infinity far away from the body. In addition, the velocity potential has to fulfil body boundary condition on the hull surface. Because the free surface condition has to be solved at the instantaneous free surface elevation around the body and the body conditions have to be solved on the instantaneous wetted surface, the boundary value problem is nonlinear.

Linearization of the free surface and the body boundary conditions with respect to the wave amplitude means that the wave amplitude is assumed to be small compared to other length dimensions of the fluid and the body. In linear frequency domain methods the body and free surface boundary conditions are linearized. When a linear theory is used, all hydrodynamic quantities are calculated up to undisturbed mean water level. Typically the solution of the linear problem is carried out in frequency domain, for example Chang (1977), Inglis and Price (1982), Iwashita and Ohkusu (1989), and Iwashita (1997). The solutions and based on the frequency domain Green functions. In Green function based methods (Neuman-Kelvin theory) only body surface is modelled by panels. The calculation is still time consuming when several different speeds, headings and frequencies are used. Usually the steady state disturbance potential is neglected, which simplifies the problem and hence makes the computations easier.

Time domain representation of the Green function allows that the nonlinear body boundary condition can be applied. This means that the perturbation potential can be solved in the actual floating position and not only at the mean water line of the ship. In time domain three-dimensional linear and nonlinear methods are presented Ferrant (1991), Lin and Yue (1991) and Sen (2002). Bingham *et al* (1994) applied transient Green function method to solve the boundary value problem in time domain and frequency domain.

In this report, theory of the wave load calculation method is given that was developed in the LAINE – project. The method is based on time domain representation of the Green function. The applied and developed method in LAINE-project is based on the Neuman-Kelvin theory and blending techniques is used to take into account the additional nonlinearities due to the incoming wave elevation in Froude-Krylov and hydrostatic restoring forces and moments. The theoretical background is the same as presented, for example Ferrant (1991), Lin and Yue (1991) and Sen (2002).

2.2 Theory

The theory is based on potential theory and hence the motion of the fluid can be expressed by a single scalar function, i.e. velocity potential. Boundary conditions are applied at the boundaries of the fluid. The nonlinear free surface boundary condition is linearized but exact body boundary condition is applied on the body surface (body nonlinear version). Calculations can be performed also with linear body boundary condition (body linear version). In addition, boundary conditions are needed at infinity and at the bottom of the sea. Two co-ordinate systems are used; space fixed co-ordinate system, x,y,z and body fixed co-ordinate system x_0,y_0,z_0. The co-ordinate systems are shown in Figure 2.1. The hydrodynamic boundary value problem is solved in the space fixed co-ordinate system. Body normals are defined as positive into the body (out of the fluid). Ship speed is U in the direction of x-coordinate and head seas is heading angle χ = 180 degrees. The six degrees of freedom body motions are surge (η_1), sway (η_2), heave (η_3), roll (η_4), pitch (η_5) and yaw (η_6) defined with respect to the space fixed co-ordinate system.

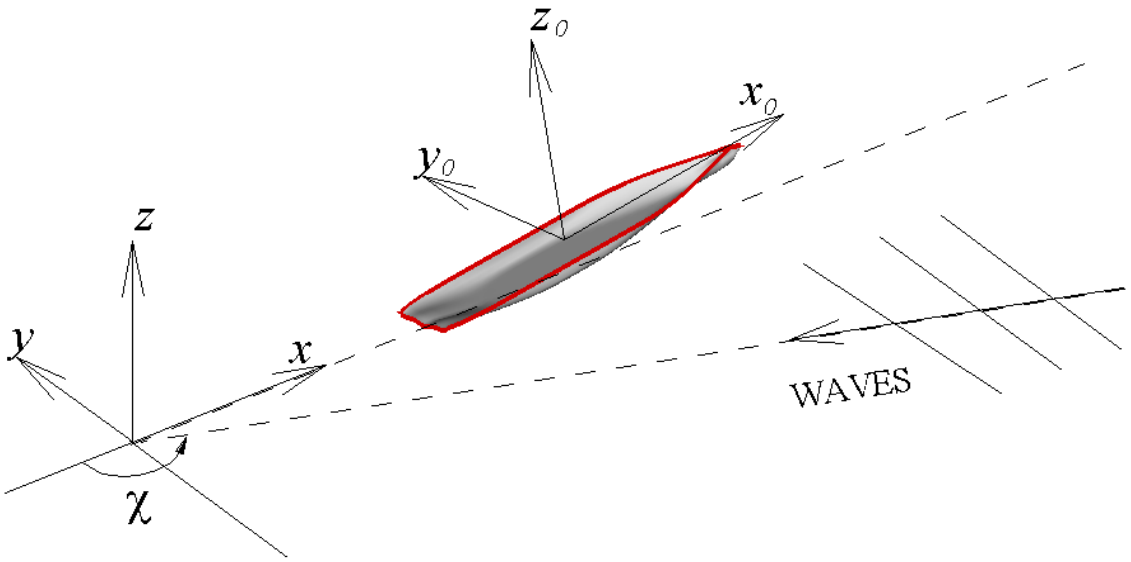

Figure 2.1. Co-ordinate system used in the time domain calculation method.

Total velocity potential can be expressed as follows:

$$\Phi = \phi + \phi_I \tag{2.1}$$

where the perturbation velocity potential is $\phi = \Phi - \phi_I$ and the velocity potential of the incoming wave is ϕ_I. The perturbation potential ϕ have to fulfil the Laplace - equation:

$$\nabla^2\phi = 0 \qquad \text{everywhere in the fluid.} \tag{2.2}$$

In addition, the velocity potentials have to fulfil the boundary conditions on body (S_B) and on the free surface. Linearized free surface boundary condition is

$$\frac{\partial^2\phi}{\partial t^2} + g\frac{\partial\phi}{\partial z} = 0 \text{ on } z = 0. \tag{2.3}$$

where t is the time and g is the gravity acceleration. The body boundary condition is given as follows

$$\frac{\partial\phi}{\partial n} = \mathbf{V}\cdot\mathbf{n} - \frac{\partial\phi_I}{\partial n} \quad \text{on body boundary } S_B. \tag{2.4}$$

Here **n** is the unit normal to body pointing out of the fluid and **V** is the instantaneous velocity of the body.

In addition, the bottom boundary condition

$$\frac{\partial\phi}{\partial n} = 0, \; z \to -\infty. \tag{2.5}$$

and the radiation condition ($r = \sqrt{x^2 + y^2}$):

$$\phi \to 0, \; r \to \pm\infty. \tag{2.6}$$

are taken into account at infinity. Furthermore, the boundary value problem has to fulfil the following initial conditions at $t = 0$:

$$\phi = 0 \text{ and } \frac{\partial\phi}{\partial t} = 0 \tag{2.7}$$

The velocity potential of the incoming wave fulfil the Laplace equation, the linearized boundary condition at the free-surface and the bottom boundary condition. The velocity potential of the wave can be given in the following form

$$\phi_I = \mathrm{Re}\left\{ i\frac{ga}{\omega} \mathrm{e}^{-i(kx\cos\chi + ky\sin\chi)} \mathrm{e}^{kz} \mathrm{e}^{i\omega t} \right\} \tag{2.8}$$

where a is the wave amplitude, ω is the wave frequency and k is the wave number.

The hydrodynamic pressure acting on the body is obtained from Bernoulli's equation

$$p_T(P,t) = -\rho\left[\frac{\partial\Phi}{\partial t} + \frac{1}{2}\left|\nabla\Phi\right|^2 + gz\right] \tag{2.9}$$

where the velocity potential is $\Phi = \phi + \phi_I$, see Equation (2.1). The hydrodynamic forces and moments of the body are

$$F_i(t) = \int_{S_B(t)} p_T(P_0,t) n_{0i} dS, \qquad i = 1,2,...,6 \tag{2.10}$$

where n_{0i} is a component of the generalized unit normal pointing into the body.

The accelerations of the body can be solved from the equation of motion. The equation of motion is expressed in body fixed co-ordinate system and co-ordinate transformations are applied between body fixed and space fixed co-ordinate systems.

The boundary value problem can be solved by applying Green's theorem and using panel method with unknown source strength distributions over the wetted body surface. The source strengths can be solved using the body boundary condition. Applying Green's theorem and using body boundary condition the source strengths can be solved from

$$
\begin{aligned}
-\frac{1}{4\pi}\iint_{S_B(t)}\sigma(Q,t)\frac{\partial G^{(0)}(P,Q)}{\partial n}dS &= -\mathbf{n}\cdot\left(\mathbf{V}-\nabla\phi_I(P,t)\right)\\
&+\frac{1}{4\pi}\int_0^t\left[\iint_{S_B(\tau)}\sigma(Q,\tau)\frac{\partial G^{(t)}(P,Q,t,\tau)}{\partial n}dS\right]d\tau\\
&-\frac{1}{4\pi}\frac{1}{g}\int_0^t\left[\int_{\Gamma_F(\tau)}\sigma(Q,\tau)\frac{\partial G^{(t)}(P,Q,t,\tau)}{\partial n}u_n U_N d\Gamma\right]d\tau
\end{aligned}
\qquad (2.11)
$$

Here G is the Green function, σ is the source strength, $P = P(x, y, z)$ is the field point and $Q = Q(x', y', z')$ is the source point. Present time is t and $\tau < t$. The normal vector $\mathbf{n}$ is located at point P, $\mathbf{n} = \mathbf{n}(P)$. The velocities u_n and U_N are three- and two-dimensional normal velocities, respectively, of the body boundary intersection at free surface at source point Q. The two normal velocities are related by $U_N = u_n/(\mathbf{N}\cdot\mathbf{n})$. The last line integral is around the body boundary at the free surface. Two-dimensional normal at waterline is $\mathbf{N}$. Once the source strengths are solved the velocity potential can be obtained from

$$
\begin{aligned}
\phi(P,t) &= \frac{1}{4\pi}\iint_{S_B(t)}\sigma(Q,t)G^{(0)}(P,Q)dS\\
&+\frac{1}{4\pi}\int_0^t\left[\iint_{S_B(\tau)}\sigma(Q,\tau)G^{(t)}(P,Q,t,\tau)dS\right]d\tau\\
&-\frac{1}{4\pi}\frac{1}{g}\int_0^t\left[\int_{\Gamma_F(\tau)}\sigma(Q,\tau)G^{(t)}(P,Q,t,\tau)u_n U_N d\Gamma\right]d\tau
\end{aligned}
\qquad (2.12)
$$

The time dependent Green function is (Wehausen and Laitone, 1960)

$$
G=\frac{1}{R}-\frac{1}{R'}+2\int_0^\infty\left[e^{k(z+z')}\sqrt{gk}\sin(\sqrt{gk}(t-\tau))J_0(kr)\right]dk \qquad (2.13)
$$

for $z < 0$, $\tau < t$ and $P(x, y, z) \neq Q(x', y', z')$ and where

$$
\begin{aligned}
R &= \sqrt{(x-x')^2+(y-y')^2+(z-z')^2}\\
R' &= \sqrt{(x-x')^2+(y-y')^2+(z+z')^2}\\
r &= \sqrt{(x-x')^2+(y-y')^2}\,.
\end{aligned}
$$

The field point is $P = (x,\ y,\ z)$ and the source point is $Q = (x', y', z')$. The time dependent Green function $G^{(t)}$ can be given in the following nondimensional form:

$$G^{(t)}(X,Y,Z,T) = \sqrt{\frac{g}{R'^3}}\hat{G}^{(t)}(\mu,\beta) \tag{2.14}$$

where the nondimensional expression is

$$\hat{G}^{(t)}(\mu,\beta) = 2\int_0^\infty \left[e^{-\lambda\mu}\sqrt{\lambda}\sin(\beta\sqrt{\lambda})J_0(\lambda\sqrt{1-\mu^2})\right]d\lambda \tag{2.15}$$

In the above equations $T = t - \tau$, $X = x - x'$, $Y = y - y'$, $Z = z - z'$ and $Z' = z + z'$. The nondimensional time is $\beta = T\sqrt{\frac{g}{R'}}$ and the nondimensional vertical coordinate is $\mu = -\frac{Z'}{R'}$. The nondimensional wave number is $\lambda = kR'$. The Green function term $\hat{G}^{(t)}(\mu,\beta)$ is shown in Figure 2.2.

In the calculation the most time consuming part is the solution of the time dependent Green function. Because of the time convolution integral the solution time is proportional to the number of panels N_P squared times the number of the previous time steps N_τ. At every time steps $N_P^2 \times N_\tau$ evaluations of the Green function is necessary in the body nonlinear solution.

Usually the time-dependent Green function is solved using series expansion together with asymptotic expansions (Newman, 1992). Applying the series and asymptotic expansions the solution domain in β-μ plane is divided in sub domains where different solution strategies are applied. Numerical integration rules, such as Filon' integral formulas have been used also for higher values of β. The time dependent Green function can be solved also using Taylor series expansion. Clement (1998) showed that the time dependent Green function is a solution of ordinary differential equation and a solution for this problem using Taylor series expansion was presented by Chuang *et al* (2007).

In the present calculation method the time dependent term $G^{(t)}$ and corresponding derivatives were solved using numerical integration. Gauss-Kronrod numerical quadrature formulas were applied to solve the time dependent terms of the Green function. In the adaptive integration, the integration interval was subdivided into smaller intervals where the estimated largest errors exist. The interval with estimated largest error was bisected and the Gauss-Kronrod rule was applied for each subinterval. The error for each interval was estimated by comparing between the result obtained by 21-point Gauss–Kronrod rule and that by ten-point Gauss rule. The numerical integration solution was compared to the series solution given in Newman (1992). The series solution was based on the series and asymptotic expansions. Series solution was performed in two parts, the Legendre function representation was applied for interval β = 0 ... 9 and the asymptotic expansion for β > 9. High numerical accuracy is needed in the series expansion solution because of the large values in the denominator and numerator if nondimensional time β is increasing. This is one reason why the Green function term solution is split in two intervals with respect to β. One advantage of the numerical integration approach is that the same solution strategy can be applied in the solution domain for all β and μ without using different solutions in different subdomains.
The time dependent Green function term $\hat{G}^{(t)}$ solved by the numerical integral rule and the series solutions are shown in Figure 2.3. The Green function term $\hat{G}^{(t)}$ is given for two different values of the nondimensional co-ordinate μ. The lines for the two different solutions are indistinguishable in the figures.

The direct numerical integration is time consuming during the simulation. On each time step Green function and its derivatives have to be solved between all of the panels. In addition the functions have to be solved also for the past time steps because of the convolution integral. The time dependent Green function is function of the co-ordinates between source and field points and between the past and present time, and it is not depend for example of the frequency of the incoming wave, heading and speed of the ship. Hence the Green function can be evaluated beforehand for several nondimensional parameters β and μ and during simulation the Green function values can be interpolated from the tabulated values.

In the developed computer application the Green function was solved beforehand and the results were stored in the file. In the beginning of the simulations the matrix $\hat{G}^{(t)}(\mu,\beta)$ was read into the computer's memory. During the simulation the Green function values were interpolated from the matrix using finite element shape functions. Nine-node quadrilateral elements were used to describe the shape functions. The pre-calculated Green function values were evaluated in constant intervals of β and μ. The pre-calculated values were modelled as global finite element mesh with nodes at β and μ. During the simulation for given β and μ the nodal values for interpolation can be easily found from the global element mesh without time consuming searching algorithms if constant size elements are used in β-μ plane.

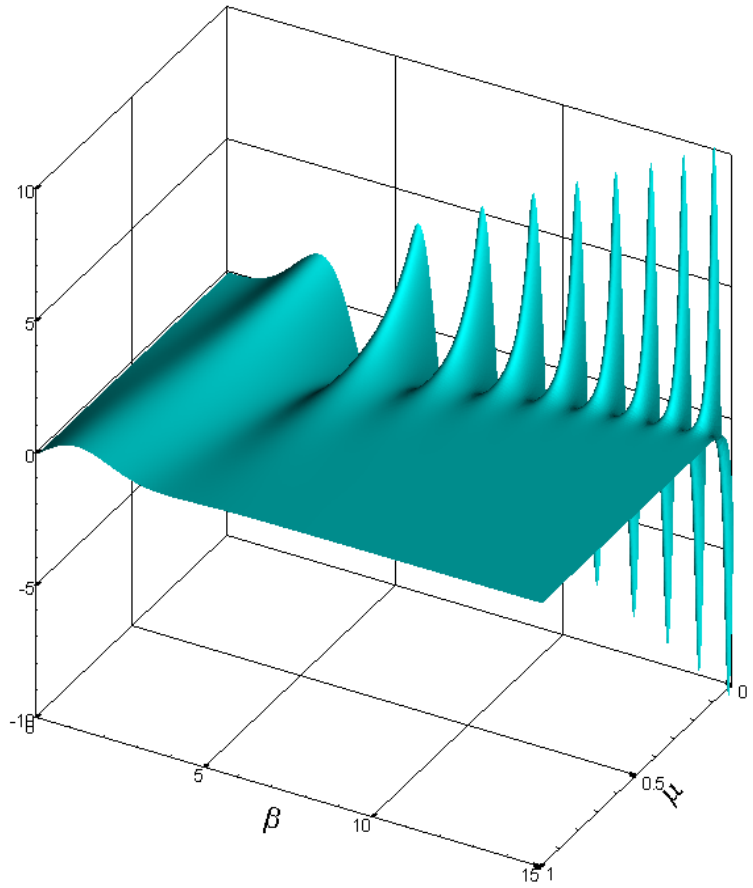

Figure 2.2. Time dependent Green function term $\hat{G}^{(t)}$ as a function of the nondimensional parameters β and μ.

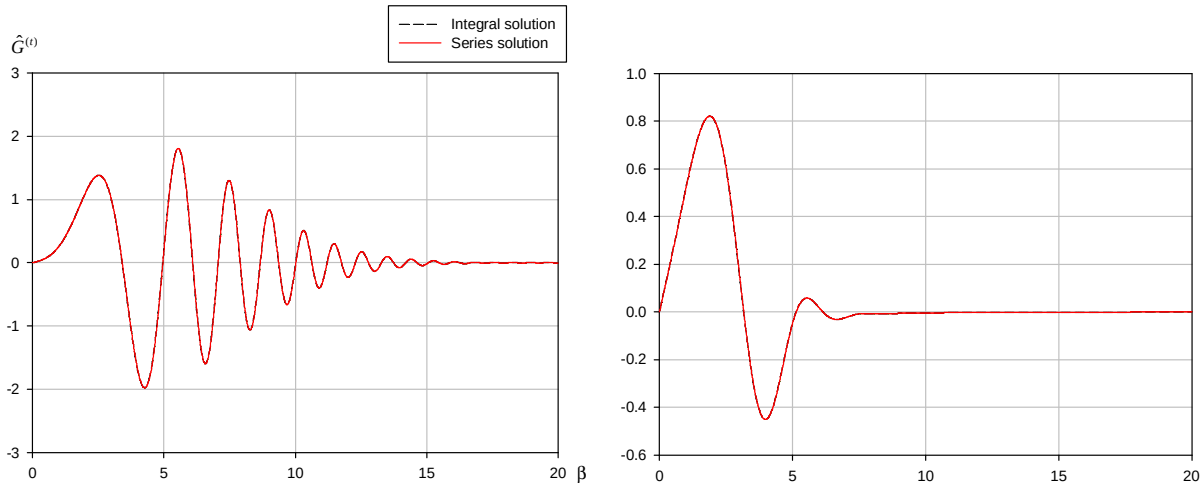

Figure 2.3. Green function term $\hat{G}^{(t)}$ given at μ = 0.1 (left) and μ = 0.5 (right). The solutions based on the numerical integration rule and series solution are shown in the figures. The lines for the two different solutions are indistinguishable.

The time derivative of the perturbation velocity potential ϕ in Bernoulli's equation (2.9) is approximated as follows

$$\frac{\partial \phi}{\partial t} \approx \frac{\phi_k - \phi_{k-1}}{\Delta t} - \mathbf{V} \cdot \nabla \phi \qquad (2.16)$$

where ϕ_k is the velocity potential at time step *k*. The solution of the time derivative of the velocity potential can be determined also by solving a separate boundary value problem defined for the time derivative of the velocity potential. This approach was presented Wu (1998) and another approach using new velocity potential definition and boundary value problem was presented in Greco (2001). Here slightly different approach is adopted defining first new velocity potential and the determining the corresponding body boundary condition that have to be solved. Hence, defining first the following velocity potential:

$$\varphi = \frac{\partial \phi}{\partial t} + \mathbf{V} \cdot \nabla \phi$$

Thus, first the velocity potential φ is solved and from the above equation the time derivative ϕ_t is obtained. The derivatives of the velocity potential ϕ are already known from the original boundary value problem. The velocity potential φ has the same solution as the normal velocity potential ϕ but different body boundary condition on S_B. The body boundary condition can be defined starting from the original body boundary condition as expressed in Wu (1998). First taking total time derivative from both sides of the body boundary condition for velocity potential ϕ:

$$\frac{d}{dt}\left(\frac{\partial \phi}{\partial n}\right) = \frac{d}{dt}\left[(\mathbf{V} - \nabla \phi_I) \cdot \mathbf{n}\right] \qquad \text{on } S_B.$$

It can be shown that (Greco, 2001)

$$\frac{\partial \varphi}{\partial n} = \frac{\partial}{\partial n}\left(\frac{d\phi}{dt}\right) = \frac{d}{dt}\left(\frac{\partial \phi}{\partial n}\right)$$

and hence

$$\frac{\partial \varphi}{\partial n} = \frac{d}{dt}\left[(\mathbf{V} - \nabla\phi_I)\cdot\mathbf{n}\right] \qquad \text{on } S_B.$$

The right hand side of the above equation can be further developed to obtain the following body boundary condition for the velocity potential φ on the body surface S_B:

$$\frac{\partial \varphi}{\partial n} = \mathbf{n}\cdot\left[(\dot{\mathbf{u}} + \dot{\boldsymbol{\omega}}\times\mathbf{r}) - (\boldsymbol{\omega}\times\mathbf{u})\right] - \mathbf{n}\cdot\left[\frac{\partial \nabla\phi_I}{\partial t} + ((\mathbf{u} + \boldsymbol{\omega}\times\mathbf{r})\cdot\nabla)\nabla\phi_I - (\boldsymbol{\omega}\times\nabla\phi_I)\right]$$

This is implicit boundary condition because of the body accelerations on the right hand side. Thus iterative solution procedure is needed in the time integration of the equation of motions. The solution has been implemented in the calculation program. Good results were obtained for example for the added mass and damping coefficients of the hemisphere presented in Kukkanen (2008b) where calculations were carried out using the normal numerical approximation for the velocity potential time derivative. An example of the direct solution of the ϕ_t compared to the approximation is presented in Figure 2.4. In the figure the heave radiation force is presented for the Seatech-D ship in irregular waves. The direct solution and the approximation are the same but some peaks and irregularities are clearly visible in the approximated solution. However, the boundary value solution should be further investigated and detail verification and validation is still needed. All of the calculations presented here were solved using the approximation for the ϕ_t unless otherwise stated.

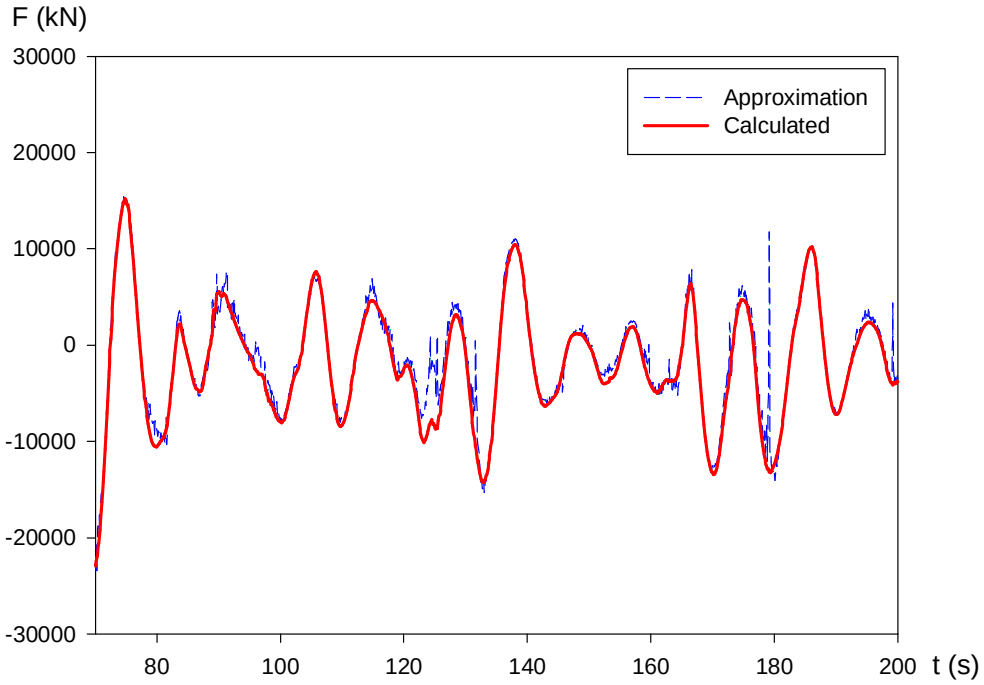

Figure 2.4. Heave radiation force based on the direct solution of ϕ_t and the approximation. Example is from irregular wave calculatios for the Seatech-D ship.

2.3 Calculation procedure

The calculation procedure is presented in Figure 2.5. The exact body boundary condition is applied on the body surface in the body nonlinear version. In the body nonlinear solution all the pressure components are calculated at the instantaneous position of the ship up to the level of z = 0. Calculations can be performed also using the linear body boundary condition (body linear version).

The program includes two options to evaluate the Green function. The Green function can be calculated beforehand or solved during the simulation. The pre-calculated version is considerably faster and it was used in all of the results presented in this report. The Green functions were determined at panel centroid or using numerical integration over panel area by Gauss quadratures.

Before the simulation the panel mesh of the hull is constructed and the basic hydrostatic calculations are carried out. The simulations are performed in the defined operational conditions in regular or irregular waves at forward or zero speed in arbitrary heading angle.

In body nonlinear solution hull surface can be re-panelised at each time step fitting the hull cross sections with cubic splines up to the water level and taking into account the ship instantaneous position. Alternatively constant panel sizes can be used and during simulation the panels are checked if they are below or above the water level.

The ship motions are solved using explicit time integration. At the present version of the program the single step Euler method or Adams type predictor – corrector methods can be used.

The nonlinearity in hydrostatic and Froude-Krylov forces and moments can be included to the solution also. The nonlinear hydrostatic and Froude-Krylov forces and moments are calculated up to the actual incoming wave elevation.

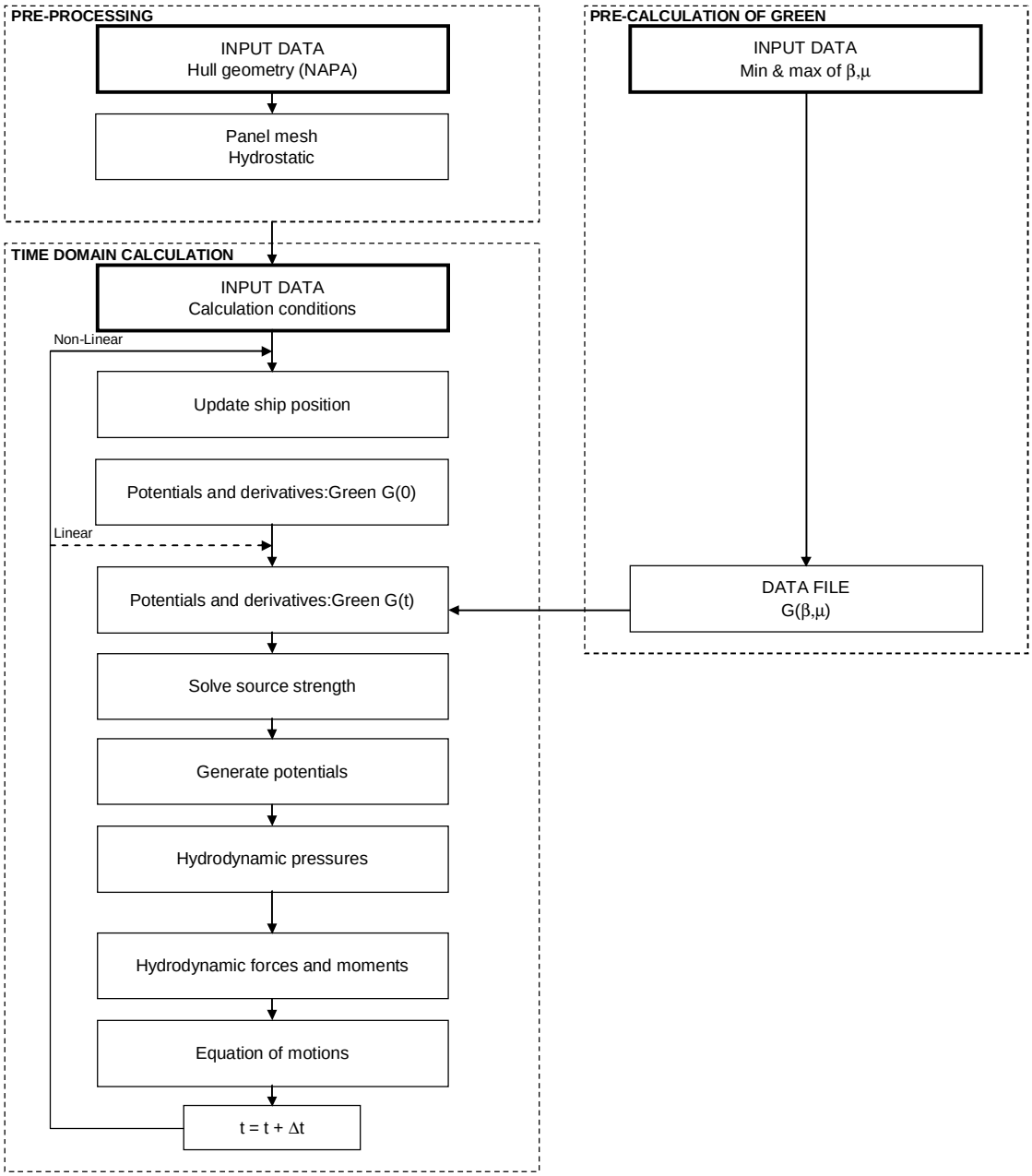

Figure 2.5. Calculation procedure.

3 Verification and validation

3.1 Simple hull forms

3.1.1 Added mass and damping of hemisphere

The solution of the hydrodynamic boundary value problem presented in the previous Chapter is carried out in time domain. Hence the solution of the conventional frequency domain added mass and damping coefficients are not needed. However, the added mass and damping coefficients can be determined applying Fourier transformation for the impulse response function. Assuming small motions the hydrodynamic pressure can be linearized and the pressure can be expressed without the velocity potential squared term. Considering only radiation pressures the contribution of the hydrostatic pressure can be neglected and the radiation force can be expressed as follows

$$L_{ii}(\tau) = \int_{S_B} \frac{\partial \phi_i}{\partial t} n_i dS \qquad (3.1)$$

where n_i is a component of a unit normal into the body. Integration is performed about mean wetted surface S_B because small motions are assumed. The unit excitation was generated using unit acceleration at the beginning of the calculation.

Added mass and damping coefficients were calculated for a hemisphere and the results were compared to the analytical solutions given by Hulme (1982). The hemisphere was modelled by panels and the number of panels for the half body was 162. Radius of the hemisphere is d and the displacement is $\nabla = 2/3\pi d^3$. Heave impulse response function $L_{33}(\tau)$ is shown in Figure 3.1. Impulse response functions are given in nondimensional form and the nondimensional time is $\tau\sqrt{g/d}$. The time step was $\Delta\tau\sqrt{g/d} = 0.157$ in the calculations. The heave added mass and damping coefficients are presented in Figure 3.2. The calculated impulse response functions correlate well with analytical solution given by Hulme (1982). The oscillation of the calculated impulse response function at the higher frequencies is due to the irregular frequencies. The irregular frequencies can be seen well from the added mass and damping figures. The first irregular frequency for heave exists approximately at $kd \approx 2.5$. The added mass peak became higher and more concentrated in the vicinity of the irregular frequency if the number of panels is increased (Lin and Yue, 1991).

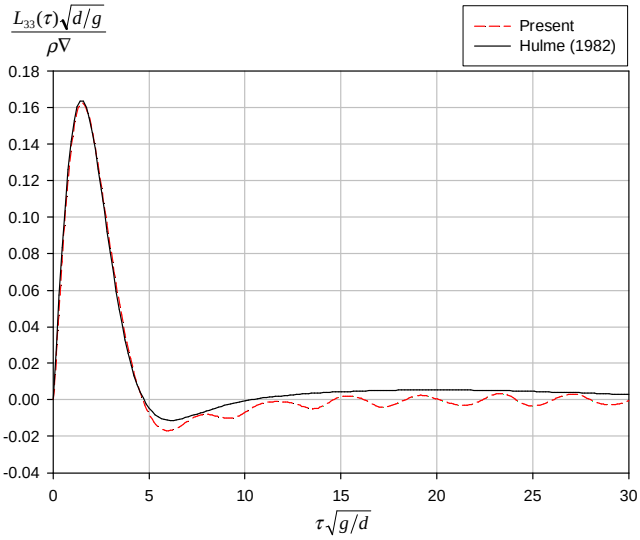

Figure 3.1. Heave impulse response function as a function of nondimensional time.

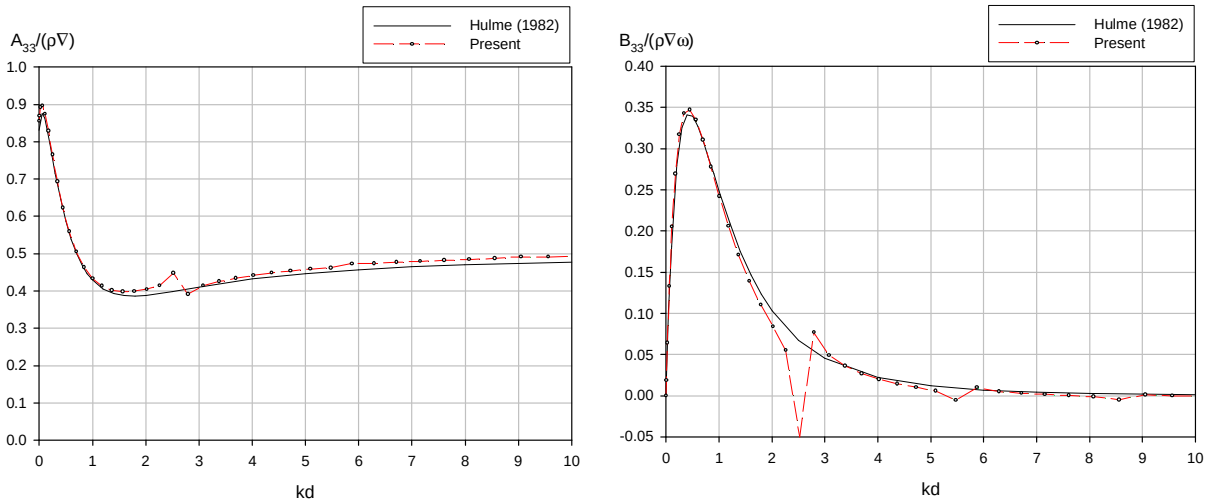

Figure 3.2. Heave added mass coefficient (left) and damping coefficient (right) as a function of nondimensional wave number.

3.1.2 Exciting forces and motions of Wigley - hull

For Wigley hull forms comprehensive model test programme was conducted by Journee (1992). Four different Wigley hull forms were tested and different responses were reported including motions and exciting forces and moments. Here the Wigley version I was used to validate the developed method. The main dimensions of the Wigley I hull are length L = 3.0 m, breadth B = 0.3 m and draught T = 0.1875 m. Calculations were carried out using the body linear and nonlinear versions of the program. Hull was re-panelised at each time step in the body nonlinear calculations fitting the hull cross sections with cubic splines. Number of panels of the half hull was 120.

The linear transfer functions of the responses were determined using harmonic analysis for the calculated time histories. In the harmonic analysis a Fourier series is fitted to the recorded data. The transfer functions or the response amplitude operators (RAO) are defined as the ratio of the response first harmonic to the wave first harmonic. The response phase angles are

defined as leads with regard to the maximum wave elevation at the centre of gravity of the ship.

Exciting heave force and pitch moment at forward speed of *Fn* = 0.20 are shown in Figure 3.3. Nondimensional wave frequency is $\omega\sqrt{L/g}$ where ω is the wave frequency and *L* is the ship length. Wave number is $k = \omega^2/g$. During the calculation the body was fixed so that the body motions were zero. Hence, the calculated forces and moments corresponds the model test conditions. In addition, the body nonlinear calculations are the same as the body linear calculations because the body motions are zero.

Heave and pitch motions at forward speed *Fn* = 0.30 are shown in Figure 3.4. In the simulations wave amplitude was *a* = 0.02 m and time step was 0.02 s. The total duration of the simulations was 20 s. Calculations were performed with the body linear and nonlinear versions. The heave and pitch motions are somewhat lower level than the model test results. The body linear and nonlinear versions gave the same type of the results. The calculated phases follow well the model test results. The motions correspond well with the measured ones in spite of the rather coarse panel mesh.

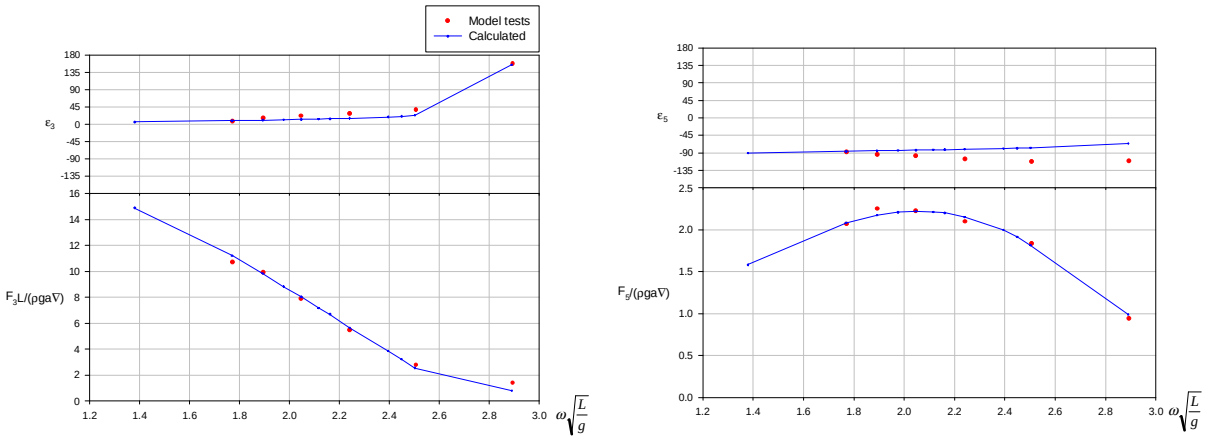

Figure 3.3. Heave and pitch exciting force and moment of Wigley I at forward speed of *Fn* = 0.20 at head seas.

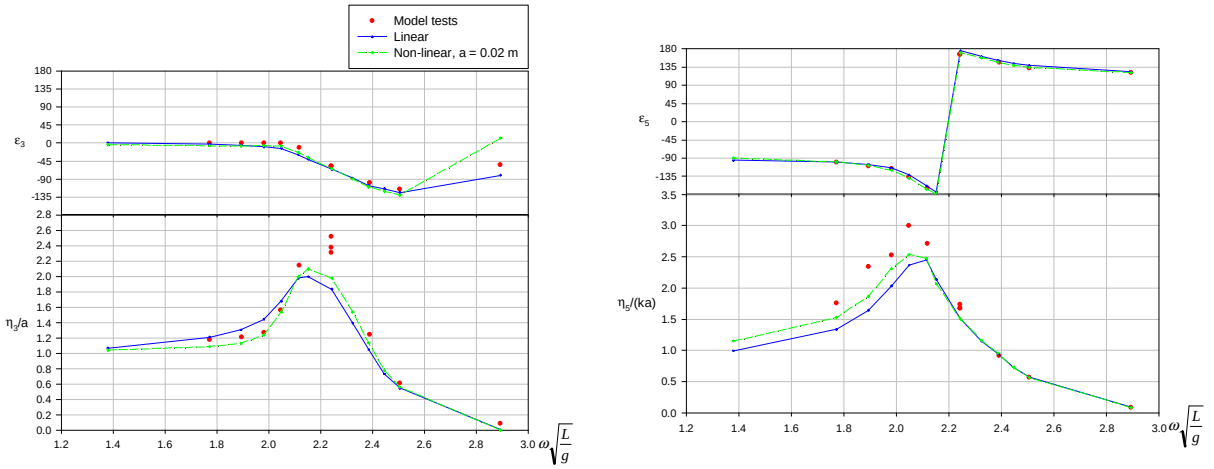

Figure 3.4. Heave and pitch motions of Wigley I in head seas at *Fn* = 0.30.

3.2 Model tests and comparison to model test results

3.2.1 Model tests

Model tests were carried out for the Seatech-D ship model in the project. The aim of the model tests was to investigate the seakeeping characteristics of the ship in waves. Seakeeping model tests consisted of the experiments in irregular and regular waves and in calm water. Tests were carried out in head waves at zero and forward speed. Main dimensions of the Seatech-D ship are given in Table 3.1 and the lines drawings of the ship are shown in Figure 3.5.

The ship model was segmented ship model and force and moment transducers were installed in two cut-off sections. The locations of the force and moment transducers are shown in Figure 3.5. The midship transducer was at frame 4 and the fore ship transducer at frame 6.5.

The main results from the model tests and comparison to calculated results are presented in this Report. The calculations in waves were performed using body nonlinear method including additional nonlinearities due to Froude-Krylov and hydrostatic restoring forces and moments. The panel mesh used in the calculations is shown in Figure 3.6. Number of panels for half ship was 648. Constant panel mesh was used in the simulations.

Table 3.1. Main dimensions of the Seatech-D ship.

Quantity	Symbol	Unit	Value
Length over all	L_{oa}	[m]	171.4
Length between pp.	L_{pp}	[m]	158.0
Breadth max. at waterline	B_{wl}	[m]	25.0
Draught	T	[m]	6.1
Displacement	∇	[m^3]	13 766
Block coefficient	C_B	–	0.55

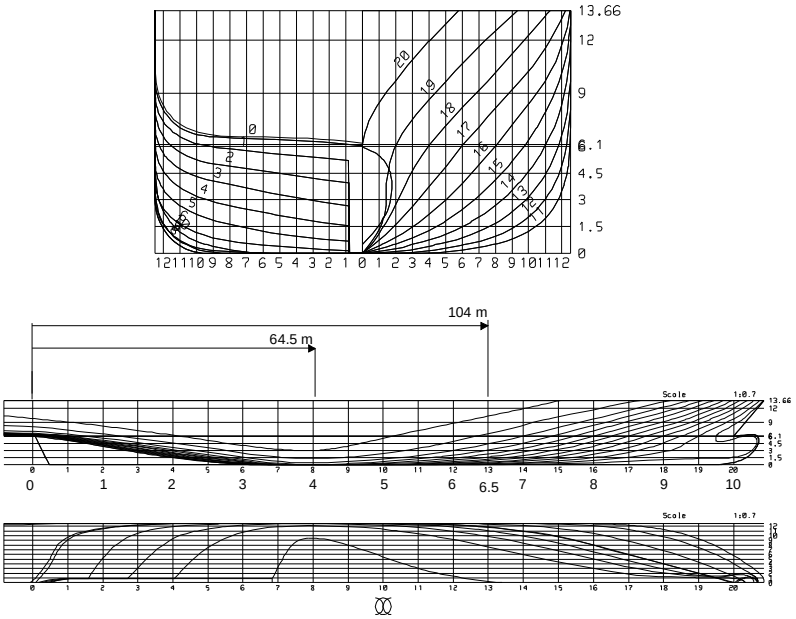

Figure 3.5. Lines drawings of the Seatech-D. The longitudinal locations of the force/torque transducers are measured from AP. The midship transducer was at frame 4 and fore ship at frame 6.5.

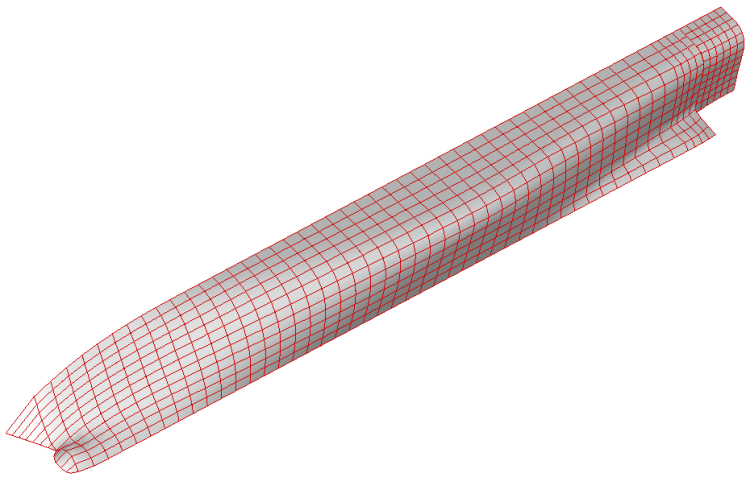

Figure 3.6. Seatech-D panel mesh in the calculations.

3.2.2 Model test results and comparison to calculations

Responses in still water were calculated in time domain as well as measured in model tests. The aim was to investigate the steady flow effects on the bending moment responses due to the pressure variation and the wave elevation. Sinkage at the centre of gravity and the vertical bending moment amidships in calm water as a function of the ship speed is shown in Figure 3.7. Froude number is $Fn = V/\sqrt{gL}$. The vertical bending moment is increasing when the speed increases. The forward speed effects induced sagging bending moment on the hull girder. The correlation between calculations and model tests is good. The time domain calculations were performed with the body nonlinear version. The calculation deviates from the model test results only at the higher speed.

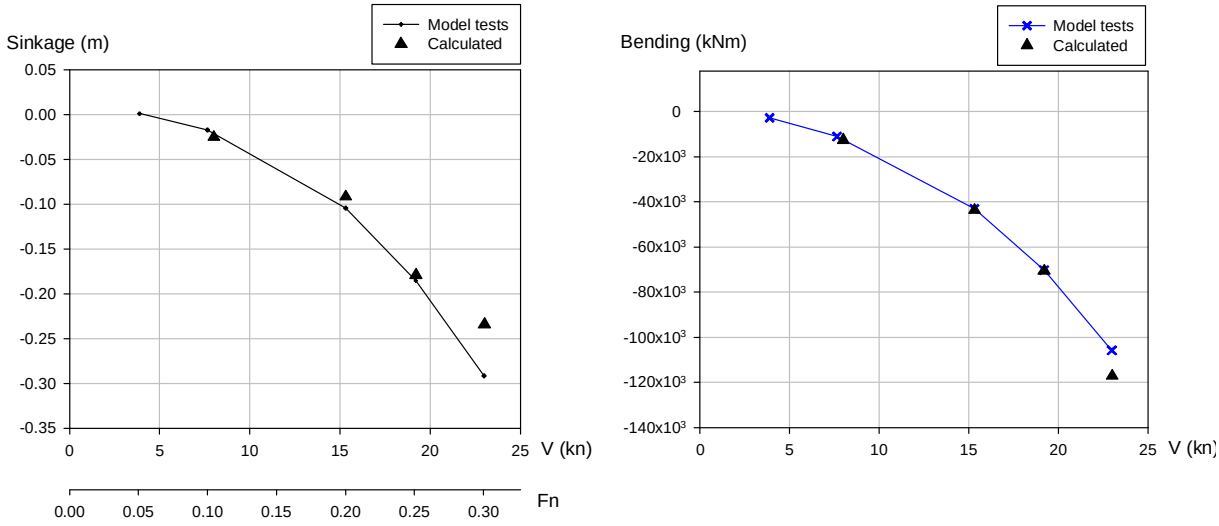

Figure 3.7. Sinkage at the centre of gravity of the ship (left) and the vertical bending moment amidships (right) in calm water as a function of the ship speed. *Fn* is Froude number.

Linear transfer functions were determined from the time domain calculations as well as from the model test results. Harmonic analyses were performed for both time histories obtained from the calculations and model tests. The first harmonic component gives the linear transfer function for the responses. Hence the given transfer functions do not show directly any nonlinearities. In the harmonic analysis a Fourier series is fitted to the recorded data. The transfer functions or the response amplitude operators (RAO) are defined as the ratio of the response first harmonic to the wave first harmonic. The phase angle of the response is defined as the first harmonic component with respect to the wave amplitude at the centre of gravity of the ship.

Linear transfer functions at zero speed in head seas are presented for the heave and pitch motions in Figure 3.8 and for the vertical shear force and bending moment in Figure 3.9. At speed of *Fn* = 0.26 the linear transfer functions are shown for the heave and pitch in Figure 3.10 and for the vertical shear force and bending moment in Figure 3.11. The model tests were carried out at different wave amplitudes. The wave amplitudes are shown in the figures. The time domain calculations were carried out at wave amplitude of a = 3 m. The calculated

results in regular waves gave good results for the ship motions comparing to the model test results. The shear forces and bending moments are well predicted by the nonlinear time domain calculations at forward speed. However differences existed at zero speed. However, the transfer functions include only the first harmonic component. Hence the transfer functions do not give correct picture of the responses that can include also nonlinearities that can be presented only by the higher order harmonic components.

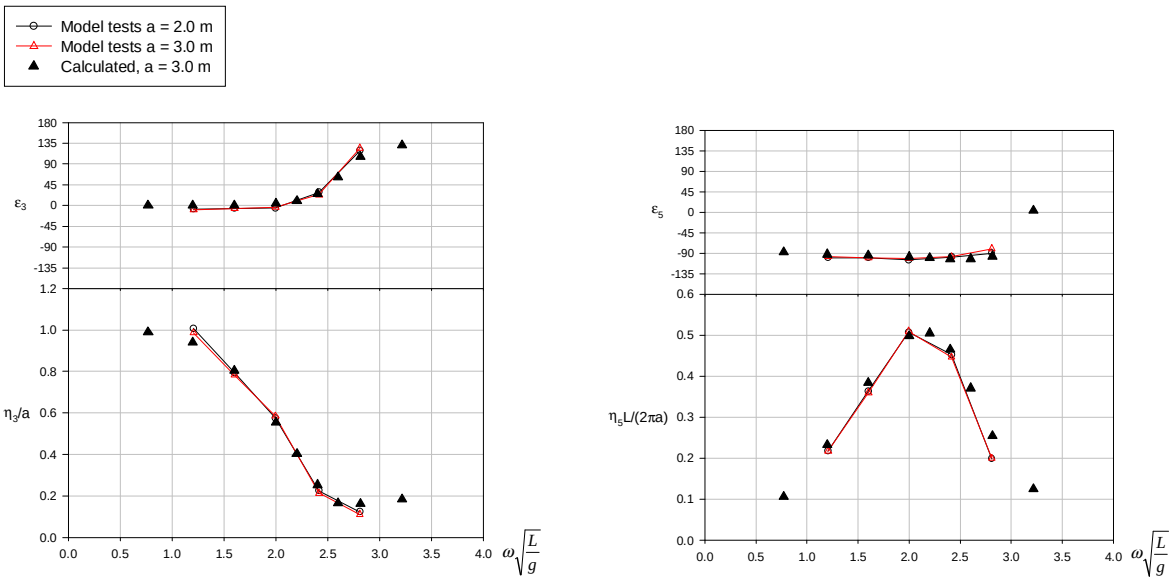

Figure 3.8. Transfer functions of heave (left) and pitch (right) at zero speed in head seas.

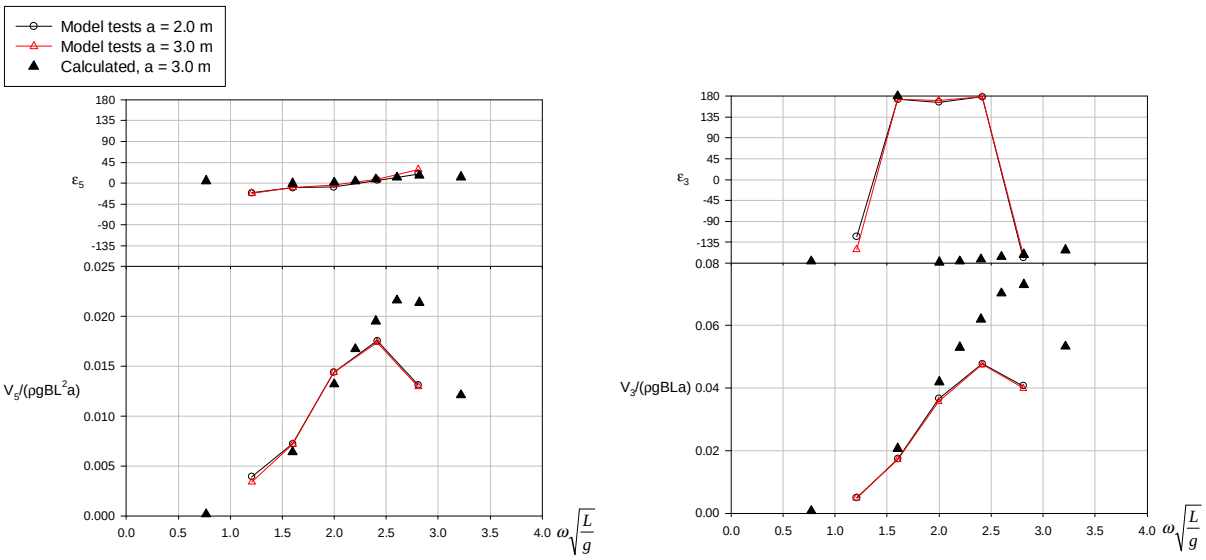

Figure 3.9. Transfer functions of vertical bending moment (left) and shear force (right) at zero speed in head seas.

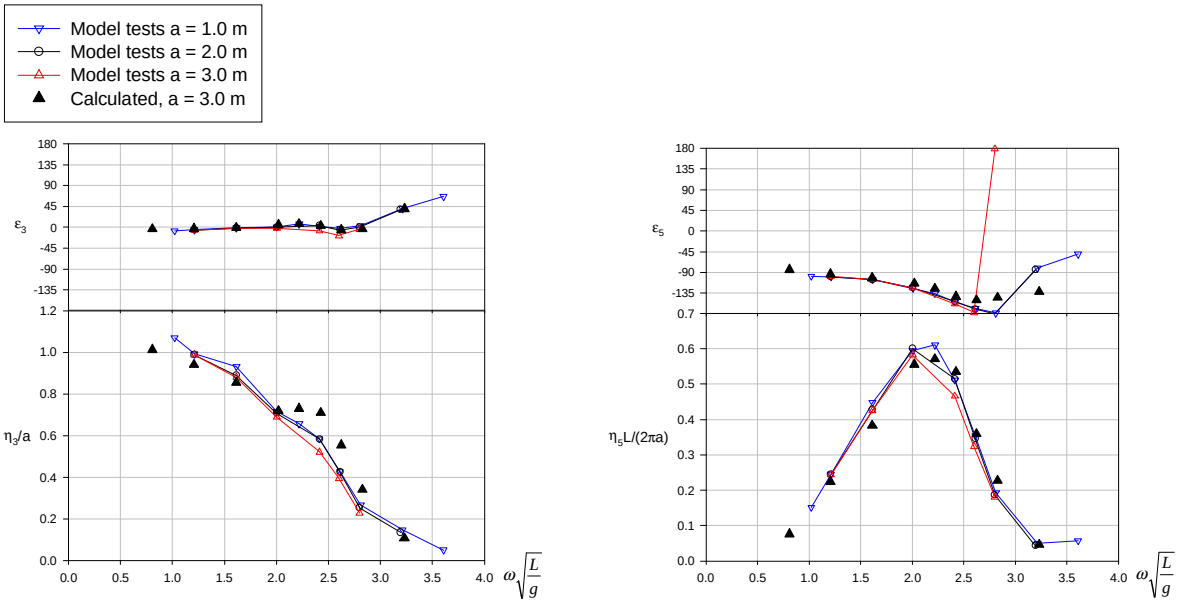

Figure 3.10. Transfer functions of heave (left) and pitch (right) at Froude number of *Fn* = 0.26 in head seas.

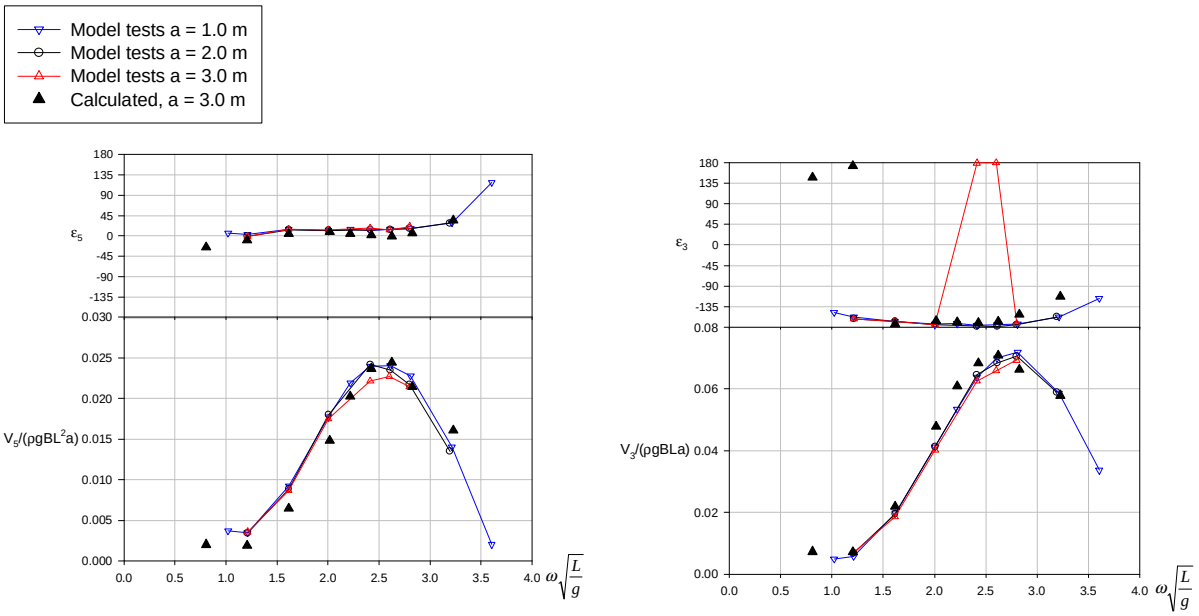

Figure 3.11. Transfer functions of vertical bending moment (left) and shear force (right) at Froude number of *Fn* = 0.26 in head seas.

The nonlinearities in the responses were investigated analysing separately the positive and negative amplitudes of the responses. The positive and negative amplitudes were analysed from the time histories of the calculated and model test results. The positive and negative amplitudes at zero speed are shown in Figure 3.12 for the heave and pitch motions and in Figure 3.13 for vertical bending moment and shear force. The same for the forward speed of *Fn* = 0.26 are shown in Figures 3.14 and 3.15. The calculated results (▲) are given together with the positive (Max) and negative (Min) amplitudes from the model tests (■). In addition

the first harmonic component (—) for heave and pitch motions based on the model test results are also shown. The calculation and model test results are given at wave amplitude of a = 3 m.

The difference between sagging and hogging bending moments as well as in the vertical shear forces could be distinguished well. The forward speed effect due the sinkage of the ship can be seen in the heave response. The difference in sagging and hogging can be partly explained by the steady flow effects due to forward speed. However, the steady bending moment in sagging has rather small effects at higher waves.

Based on model test results in regular waves the hogging moment was well predicted at zero speed and at the forward speed. The sagging moment was well predicted at forward speed but the calculated results deviated from the model test results at zero speed. Sagging was overestimated roughly about 10...20 % at zero speed. The difference can be due to the flat stern bottom close to water line. The rapid change in geometry due to the relative motions is challenging in the calculations. Better results would be obtained if the number of panels was increased and smaller panel sizes were used.

The given positive and negative amplitudes from regular wave tests and calculations were obtained directly from the time histories. The time histories of the responses include also local peaks and valleys between the global ones. Hence the given figures with the maximum and minimum amplitudes do not give the whole picture of the behaviour of the responses in regular waves.

The calculation model and the model test ship had some differences in the mass distributions. The locations of given bending moments and shear forces were also slightly different. However the differences were rather small and the differences do not explain the deviations between the model test and calculation results at zero forward speed case.

Snap shots for stern up and down in the model tests at zero speed are shown in Figure 3.16. The bow up and down case is shown in Figure 3.17 at forward speed of ship, Fn = 0.26. At zero speed the stern slamming is clearly visible as well as rather severe bow slamming if the ship has forward speed.
Time histories of the vertical bending moment from the model tests and from the time domain simulations are shown in Figure 3.18 for two different wave amplitudes, a = 1 m and a = 3 m. The forward speed is Fn = 0.26 in head seas and the nondimensional wave frequency is $\omega\sqrt{L/g}$ = 2.6 (λ/L = 0.9). In addition, the linear frequency domain prediction is also shown at the wave amplitude a = 3 m.
The position of the ship from the time domain simulations with respect to incoming wave as well as the snap shot pictures from the model tests are shown in Figures 3.19 and 3.20 at the zero forward speed. The first figure shows the bow entry into wave and the second one shows stern impact. In slamming problems the correct free surface elevation during the water entry is important in order to obtain reliable predictions for the impact pressures. Impact can occur at bow as shown in Figure 3.19 or at the flat stern bottom shown in Figure 3.20. It can be seen that the free surface elevation at the bow impact include significant water spray deformation or jet flow due to high water flow velocities at the body and free surface intersection. However, inside of the jet flow the pressure is close to the atmospheric pressure and the influence on the responses is insignificant. In Figure 3.20, the free surface elevation at the stern is rather moderate and the submergence of the body in calculations is similar as in the model tests. However, in the flat bottom impact the local pressures can be very high but it has not necessarily significant contribution on the global forces, i.e. the duration of impact is short

and local so that the total impulse is moderate. The sagging moment is lower at the zero speed than at the forward speed case in spite of the stern slamming.

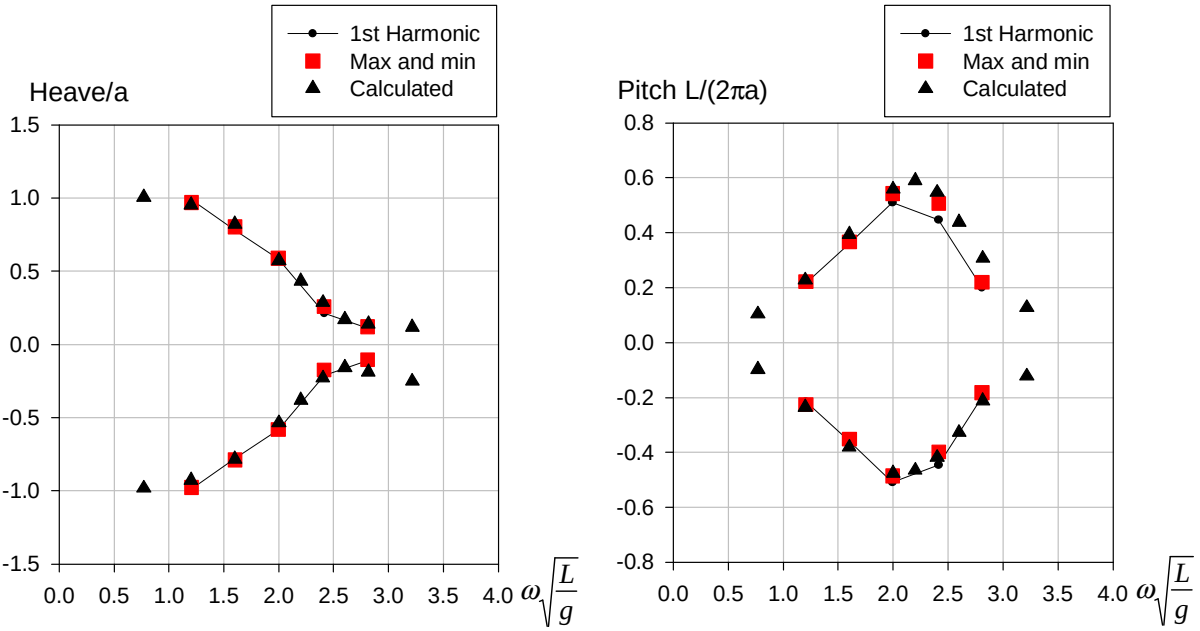

Figure 3.12. Positive and negative amplitudes of the heave (left) and pitch (right) at zero speed in head seas. Wave amplitude was 3 m in model tests and calculations.

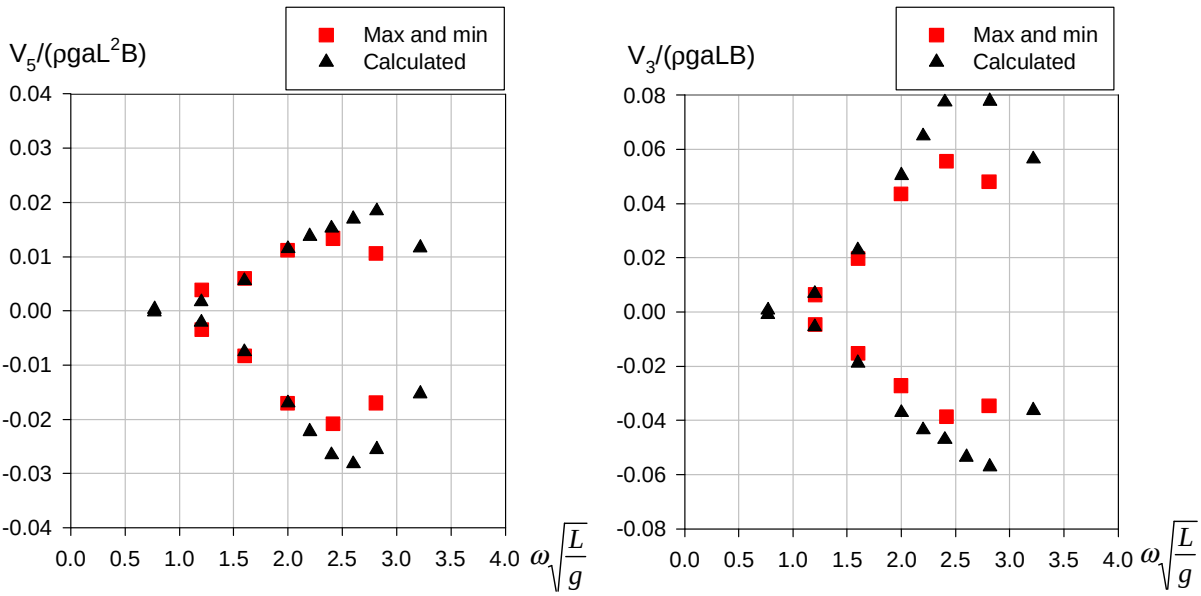

Figure 3.13. Positive and negative amplitudes of the vertical bending moment (left) and shear force (right) at zero speed in head seas. Wave amplitude was 3 m in model tests and calculations.

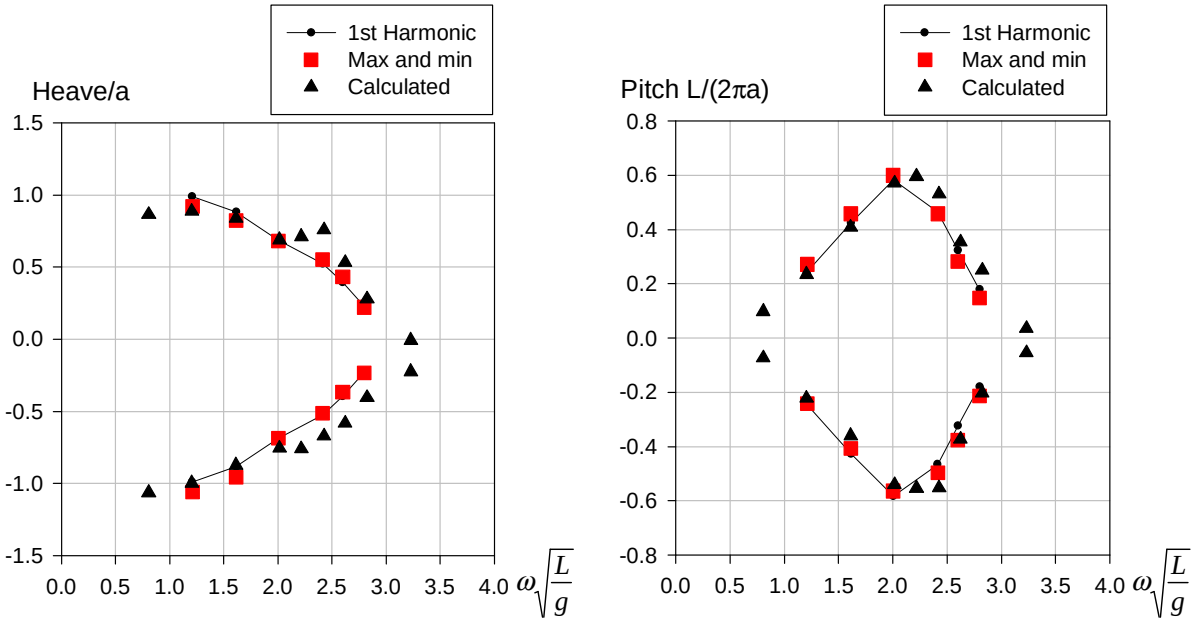

Figure 3.14. Positive and negative amplitudes of the heave (left) and pitch (right) at speed of *Fn* = 0.26 in head seas. Wave amplitude was 3 m in model tests and calculations.

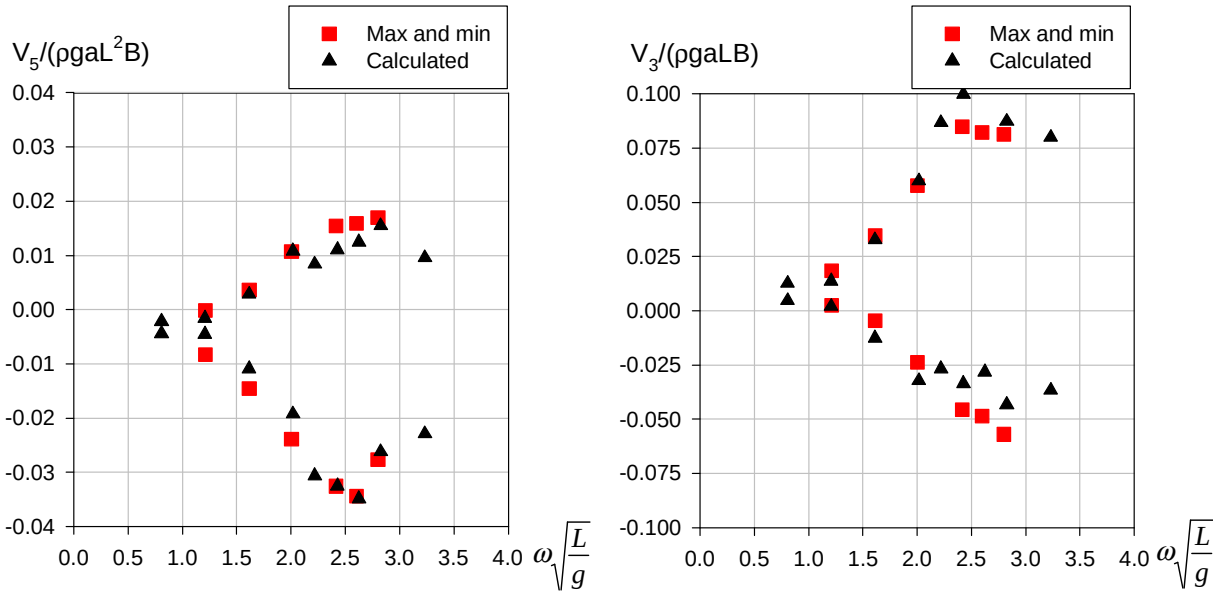

Figure 3.15. Positive and negative amplitudes of the vertical bending moment (left) and shear force (right) at speed of *Fn* = 0.26 in head seas. Wave amplitude was 3 m in model tests and calculations.

Figure 3.16. Stern of the Seatech-D model in hogging (left) and sagging (right) conditions in regular head waves at zero speed, ω = 0.60 rad/s and wave amplitude *a* = 3.0 m in full scale.

Figure 3.17. Bow of the Seatech-D model in hogging (left) and sagging (right) conditions in regular head waves at zero speed, ω = 0.60 rad/s and wave amplitude *a* = 3.0 m in full scale.

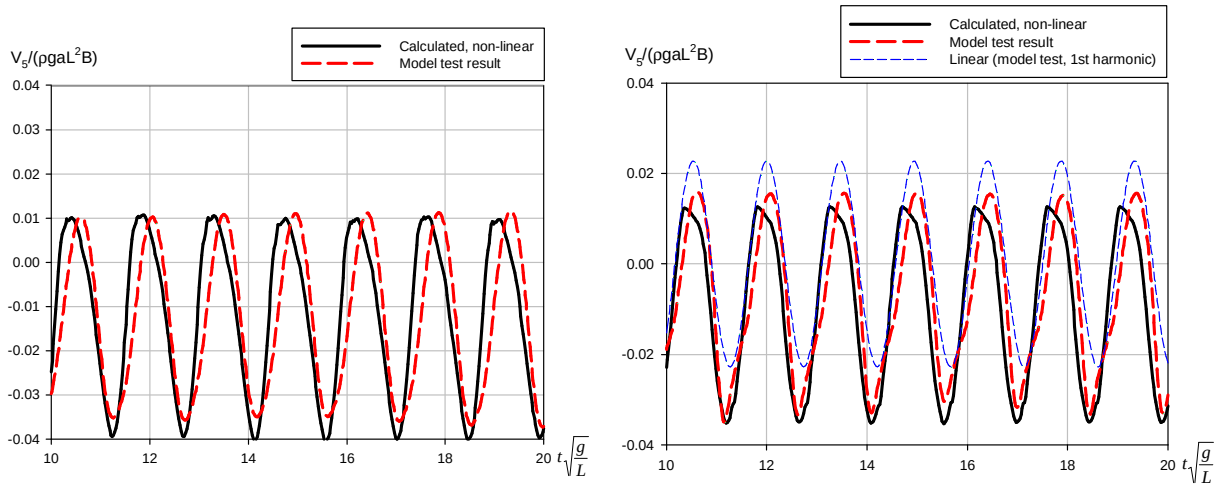

Figure 3.18. Non-dimensional vertical bending moment from model tests and calculations for the wave amplitude of *a* = 1 m (left) and *a* = 3 m (right). The nondimensional wave frequency is $\omega\sqrt{L/g}$ = 2.6 (λ/L = 0.9) and the speed is *Fn* = 0.26 in head seas. At the wave amplitude *a* = 3 m the linear 1st harmonic component is shown also.

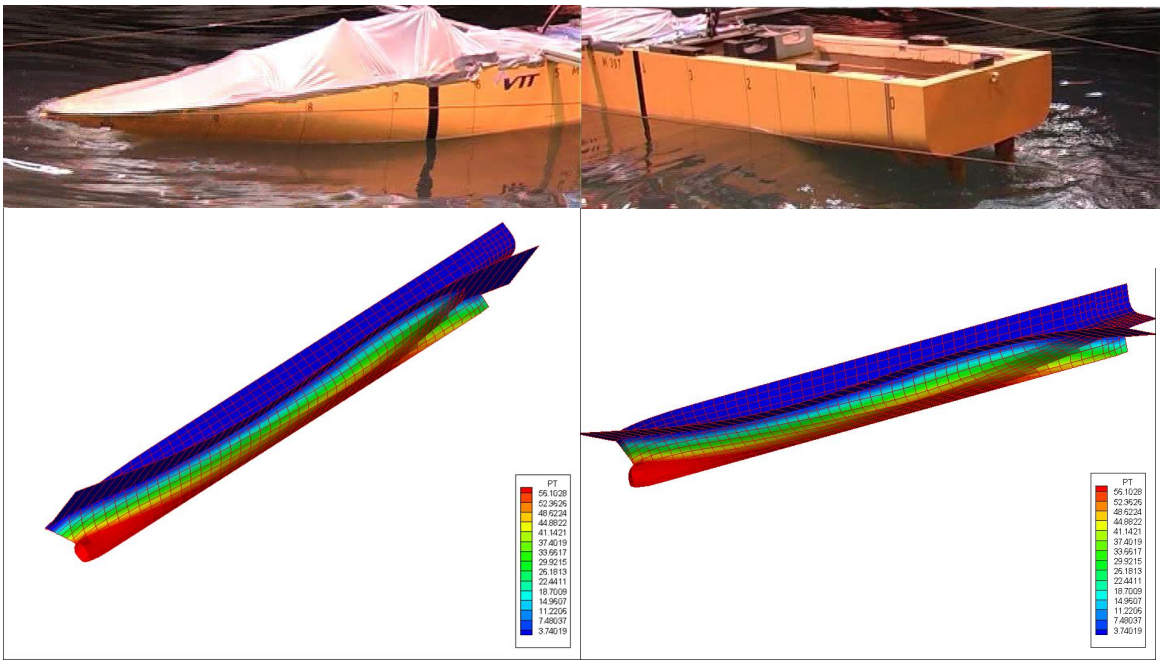

Figure 3.19. The bow down and stern up position of the ship with respect to the incoming wave in calculations and model tests, wave amplitude a = 3 m, $\omega\sqrt{L/g}$ = 2.4 and Fn = 0.0.

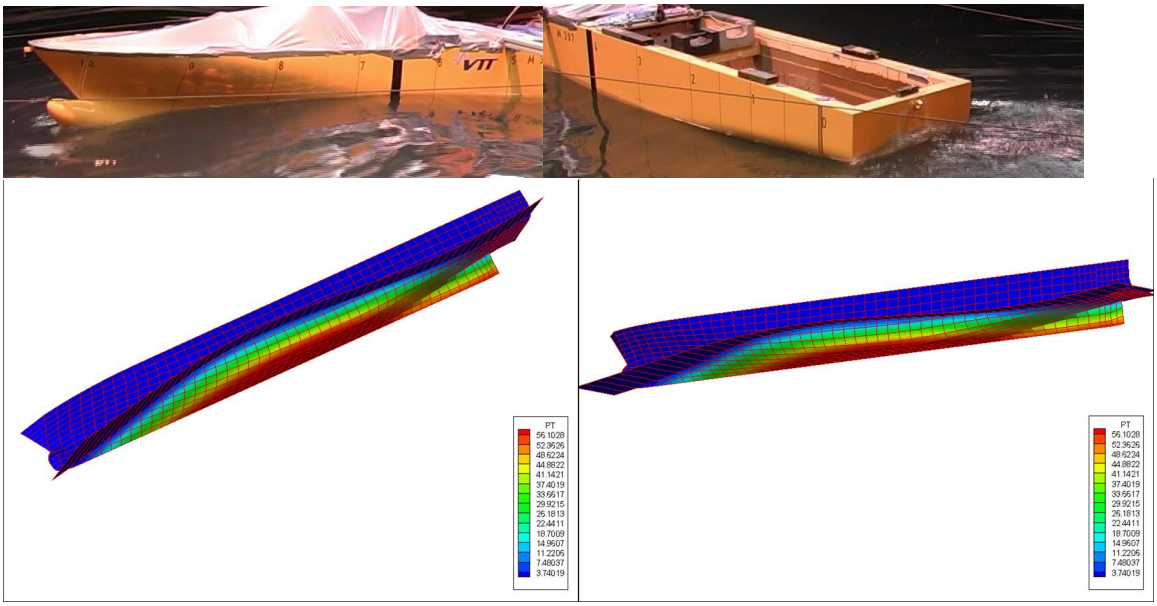

Figure 3.20. The bow up and stern down position of the ship with respect to the incoming wave in calculations and model tests, wave amplitude a = 3 m, $\omega\sqrt{L/g}$ = 2.4 and Fn = 0.0.

4 Wave load predictions

4.1 Design load predictions

In order to obtain extreme value predictions for responses it is necessary to apply probabilistic methods in the analyses due to the random nature of the ocean waves. Stochastic methods in linear frequency domain approaches are well known and widely used. Short and long-term distributions of responses can be easily determined using linear superposition principle and using spectral moments in order to obtain necessary statistical properties of the response. However, the extreme value predictions from the time domain simulations are not so well establish and usually the probabilistic distribution function of the response peaks are not known. Peak distribution is probability function of the maximum values that occur in sample data. The single extreme value is the maximum of all of the maximum peaks. However, the extreme value can vary between different sample time histories even if they are simulated in the same conditions, for example in the same sea states. This is due to the random nature of the irregular waves. Hence, the extreme value for one sample follows its own probability distribution. The probability distribution of peaks and the probability distribution of extremes are illustrated in Figure 4.1. The most probable extreme value is defined as an extreme value where the extreme value distribution has the most probable value. However, the exceedance probability of this most probable value can be rather high. In some applications the extreme value is defined using so called risk parameter or safety factor that defines the probability level where the extreme value can be exceeded, for example using 1% exceedance probability level for the extreme value.
Stochastic methods and different probability density functions for nonlinear responses in time domain were studied Wang and Moan (2004). They applied Weibull, Generalized Gamma, and Pareto distributions for time history data of nonlinear bending moments in waves. Here Weibull distribution function is used to determine the extreme values for responses in short-term sea states.

The analysis flow chart is shown in Figure 4.2. First, the n-year wave in terms of contour plot (Baarholm and Moan, 2001) of wave heights H_s and wave periods T_z are determined for the sea area where the ship will operate. In addition the speed profile as well as the headings with respect to waves should be estimated where the maximum responses can occur. The short-term predictions at different sea states defined by the H_s-T_z contour plot of the n-year waves are determined using linear frequency domain methods. The linear most probable extreme value (MPEV) is determined for the response at each sea state. Nonlinear simulations in the irregular waves are conducted in the sea state where the linear predictions get the maximum value for the response in the question. From the time domain simulations the MPEV can be defined using the Weibull distribution. This is rather straightforward for wave induced responses that can be directly obtained from the simulations such as for ship motions or hull girder loads. However, in detail structural analysis the finite element model is used and the loads are given as hydrodynamic pressures. Hence the stresses are usually determined at one time instant and the probabilistic predictions for stress responses are not defined. The worst condition in structural analysis can be defined for example using design wave approach where regular wave is determined that gives the same response as the reference response that can be for example vertical bending moment amidships.

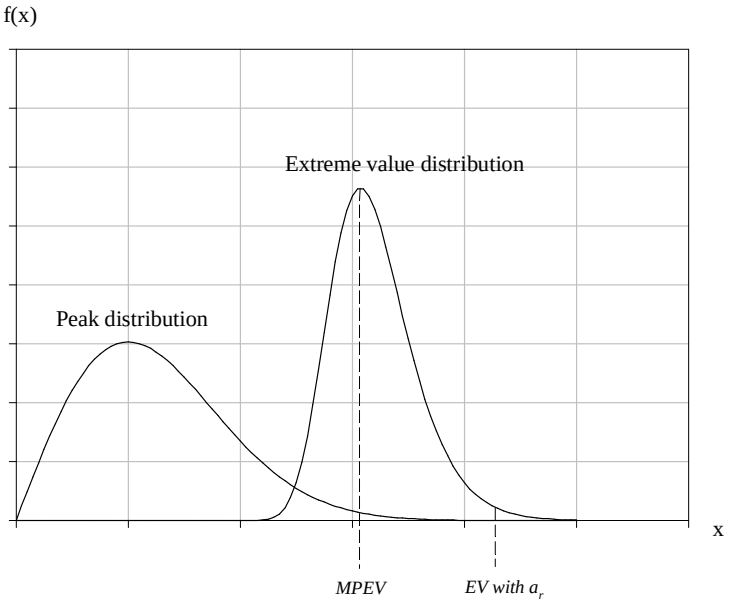

Figure 4.1. An example of peak distribution and corresponding extreme value distribution. The most probable extreme value (MPEV) and the extreme value with risk parameter a_r (EV with a_r) are also presented in the figure.

Wave scatter diagram Hs-Tz contour plot **n-year sea state Hs-Tz** **Operational profile of the ship:** speeds, headings, etc.	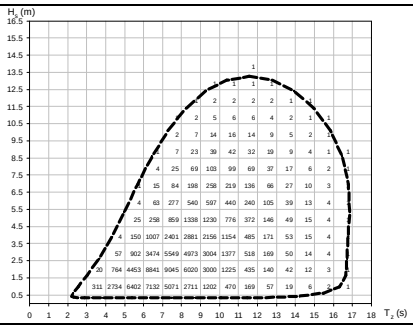
Linear frequency domain transfer functions Short-term predictions (MPEV) for different Hs-Tz in contour plot	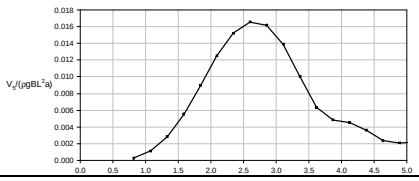
Nonlinear time domain simulations Irregular wave Hs & Tz where linear max MPEV **⇒ Nonlinear max & min MPEV predictions for response**	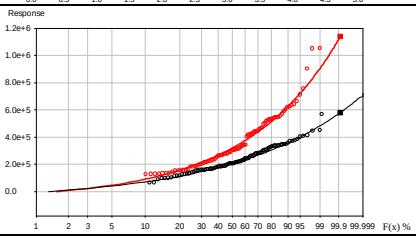
Nonlinear time domain pressures from regular waves Regular waves based on design wave approach	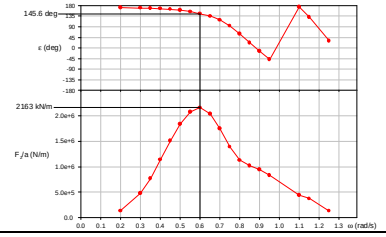

Figure 4.2. Flow chart of the analysis procedure.

4.2 Application of design load predictions for case ships

In this Chapter examples are given to determine the design wave load predictions for the Seatech-D ship.
It was assumed world wide operation of the ship but the high waves can be avoided changing the route. To take into account heavy weather avoidance in the design wave predictions the operational limit for wave height can be defined by re-scaling the Weibull distribution (Baarholm and Moan, 2001). The rescaling means that the extreme wave height will be limited to some realistic wave height where the ship can safely operate. Design waves of 1- and 20-year and 20-year wave with wave height limit of 10 m are shown in Figure 4.3. The 10 m limit is based on the re-shaping of the Weibull distribution of the wave heights. The n-year waves are based on the World Wide Trade scatter diagram (DNV, 2005). The irregular wave results given in this Chapter corresponds to the 20-year wave with H_s limit of 10 m. Irregular long-crested waves were described using the Pierson-Moskowitz wave spectrum.

For the Seatech-D ship model, linear frequency domain calculations were applied first in order to determine the linear predictions of the most probable extreme value (MPEV) for the vertical bending moment and to obtain the worst sea state that maximise the response. The time domain simulations are still time consuming and hence the linear approach was used to get approximations for the responses in several different irregular sea states. The time domain simulations were carried out in the sea state that gave the maximum linear MPEV for the vertical bending moment amidships. The linear frequency domain predictions for the MPEVs were calculated along the H_s-T_z contour that was based on the 20-year wave limited to the re-shaped distribution at $\hat{H}_s$ = 10 m. The maximum linear MPEV will be get in wave height of H_s = 9.4 m and wave period T_z = 8.5 s. The time domain simulation was carried out in this sea state. An example of the time history of the vertical bending moment amidships is shown in Figure 4.4.The significant wave height was H_s = 9.4 m and the zero crossing period T_z = 8.5 s.

In nonlinear predictions the Weibull distributions were applied in order to determine the MPEV for different responses. Weibull distributions are given for the vertical bending moment in Figure 4.5. The difference in the sagging and hogging moment can be distinguished well. Applying the probabilistic approaches for the simulated time histories it is important to define also what is the sufficient length of the simulation time. The Weibull distributions were here estimated using the mean and standard deviation of the peaks. Thus the simulation length should be long enough that these parameters are stabilised. The simulation length was 15 min in the present studies.

The MPEVs for the wave, heave, pitch and vertical bending moment in three hours sea state are given in Table 4.1. The linear frequency domain as well as the nonlinear time domain results are given in the table. The time domain calculations in irregular waves gave the predictions for the hogging and sagging bending moments 581 MNm and 1139 MNm, respectively. According to Det Norske Veritas rules the sagging wave bending moment is 970 MNm and hogging 773 MNm. The ratio of calculated and rule sagging moment is 1.17 and for hogging the same is 0.75. Thus the rule gives lower moment for sagging and higher for hogging. At zero speed and H_s = 9.4 m the ratio of calculated sagging/hogging is 2.0. On the other hand the rule gives 1.3 for the sagging hogging ratio. Hence the rule gives lower

estimate for the sagging and hogging ratio. However, these results are based only one irregular sea state simulations. Other sea states should be studied also as well as the forward speed cases. In addition the comparison to model test results showed that the calculated predictions in irregular waves at zero speed have rather large uncertainties and the calculation over estimated the responses. Results of the model test comparison are given in next Chapter.

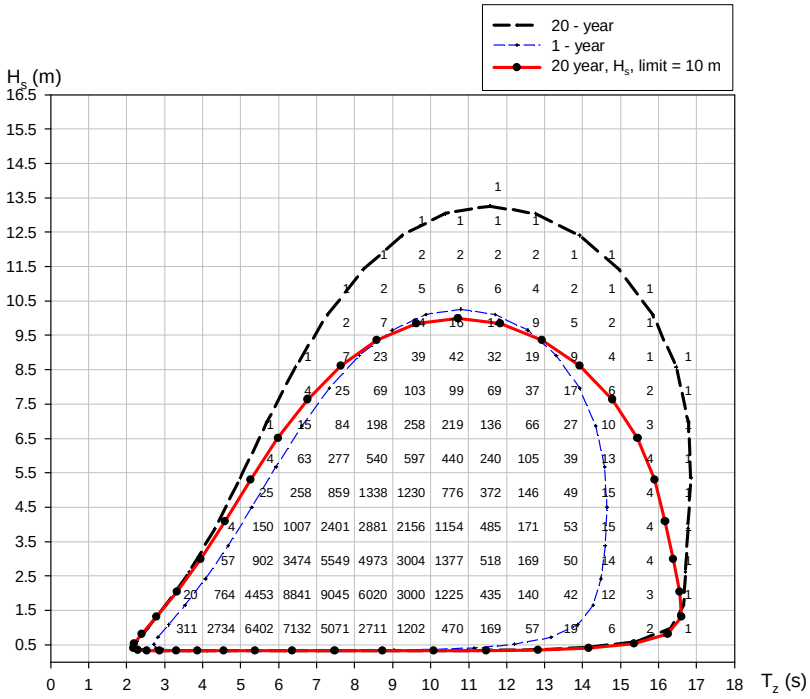

Figure 4.3. Contour plot of H_s-T_z and scatter diagram. Wave scatter diagram is based on data given by DNV (2005) for World Wide Trade. The occurrences of H_s-T_z are given as parts per 100 000.

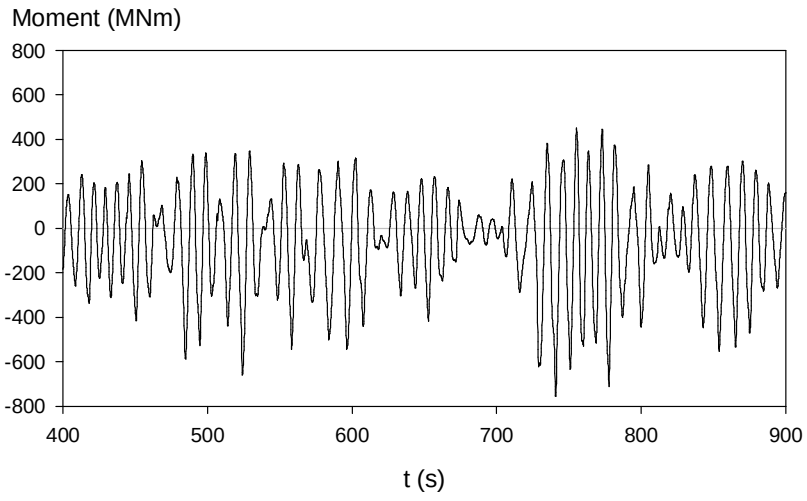

Figure 4.4. Time history example from the time domain simulation in irregular head waves at zero forward speed, H_s = 9.4 m and T_z = 8.5 s.

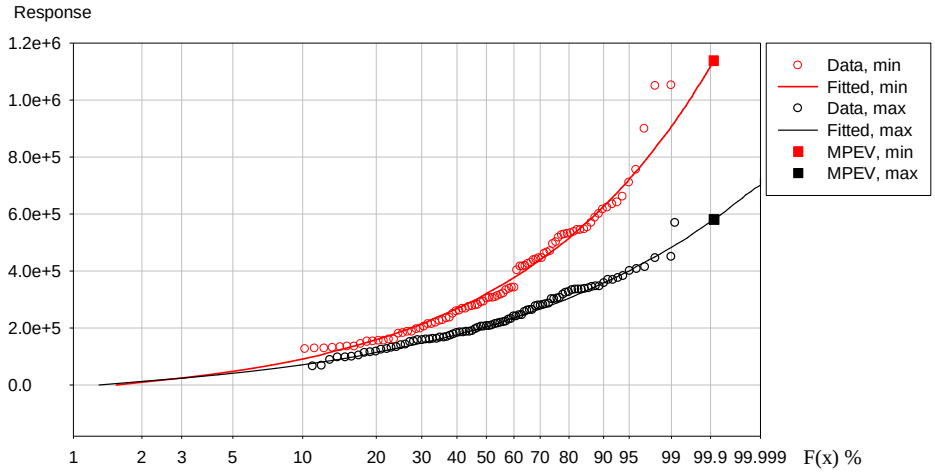

Figure 4.5. Calculated vertical bending moment amidships (kNm), H_s = 9.4 m and T_z = 8.5 s, in head seas and at zero forward speed.

Table 4.1. The most probable extreme values in sea states of three hours, H_s = 9.4 m and T_z = 8.5 s, in head seas at zero forward speed.

Response	**Linear Frequency domain**	**Nonlinear Time domain Maximum**	**Nonlinear Time domain Minimum**
Wave (m)	± 8.9	9.6	–9.5
Heave (m)	± 3.6	4.1	–3.5
Pitch (deg)	± 7.7	9.8	–7.3
Bending (MNm)	± 643	581	–1139
Shear (MN)	± 15	25	–15

4.3 Comparison to model test results

Model tests were carried out in irregular head waves at forward speed and at zero speed in different sea states. The calculations were performed also in the same conditions and the calculated results were compared to the model test results. The most probable extreme values (MPEV) of the response amplitudes were determined from the nonlinear time domain calculations as well as from the results from the model tests. Both predictions were based on the fitted Weibull distributions. The predictions were defined for the sea state duration of three hours. The MPEVs were determined for the wave, heave, pitch, heave acceleration at centre of gravity, vertical bending moments amidships and vertical shear force at fore ship.

In Table 4.2 the MPEVs are given for the response amplitudes at forward speed of 19.1 knots in the sea state of H_s = 5.0 m and T_z = 8.5 s. The peak distributions of the response amplitudes from the model test and the calculations are presented in Figure 4.6 for the vertical bending moment amidships and for the vertical shear force at fore ship. The forward speed results correlate well with the model test results.

At zero speed, the first calculations gave rather poor correlation between the model test and calculated results. Typically the calculations over predicted the responses, especially the vertical bending moments and shear forces. Hence the MPEV predictions presented in previous Chapter are also conservative estimates and rather large uncertainties can exist in the results. It was noticed that the calculated results have clear discontinuities in the time histories. The differences in calculations and model tests can be due to the flat aft bottom close to water line. The rapid change in geometry due to the relative motions of the ship in waves is challenging in the calculations. In the model tests it was observed slamming impacts at stern.
The zero forward speed calculations were repeated applying improved methods and using more accurate calculation parameters. The new calculations were performed using 2×2 point integration rule instead of the midpoint rule and using smaller panel sizes at aft body. In addition the time derivative of the velocity potential ϕ_t was solved directly using the boundary value problem approach.
The model test and calculated results for the MPEVs are given in Table 4.3 in sea state of H_s = 9.0 m and T_z = 10.5 s at zero forward speed. The peak distributions from model test and calculation are presented in Figure 4.7.
The improved calculations gave rather good results and clearly better than the original calculations. The global hull girder loads are somewhat overestimated comparing to the model test results. On the other hand, the calculation time is considerably longer because of the higher order integration rule. However, the calculations gave promising results and the accuracy of the calculated results was significantly improved at zero forward speed for the hull form with flat stern bottom. Systematic calculations and further investigations should be carried out to investigate the effect of the different calculation parameters as well to investigate the theoretical approaches to model the physical phenomena correctly. In addition the calculation time in irregular waves should be longer in order to get larger number of peaks that will improve the MPEV predictions.

Table 4.2. The most probable extreme values (MPEV) of the response amplitudes in the sea states of three hours, H_s = 5.0 m and T_z = 8.5 s, speed 19.1 knots.

U = 19.1 kn, 180° H_s = 5.0 m, T_z = 8.5 s	**Model test Maximum**	**Calculation Maximum**	**Model test Minimum**	**Calculation Minimum**
Wave (m)	6.0	5.3	–4.7	–5.0
Heave (m)	2.6	2.4	–2.4	–2.3
Pitch (deg)	4.5	4.2	–5.1	–4.1
Heave acceleration (m/s^2)	1.7	2.0	–2.1	–1.8
Bending (MNm)	401	399	–557	–564
Shear (MN)	12	13	–10	–7

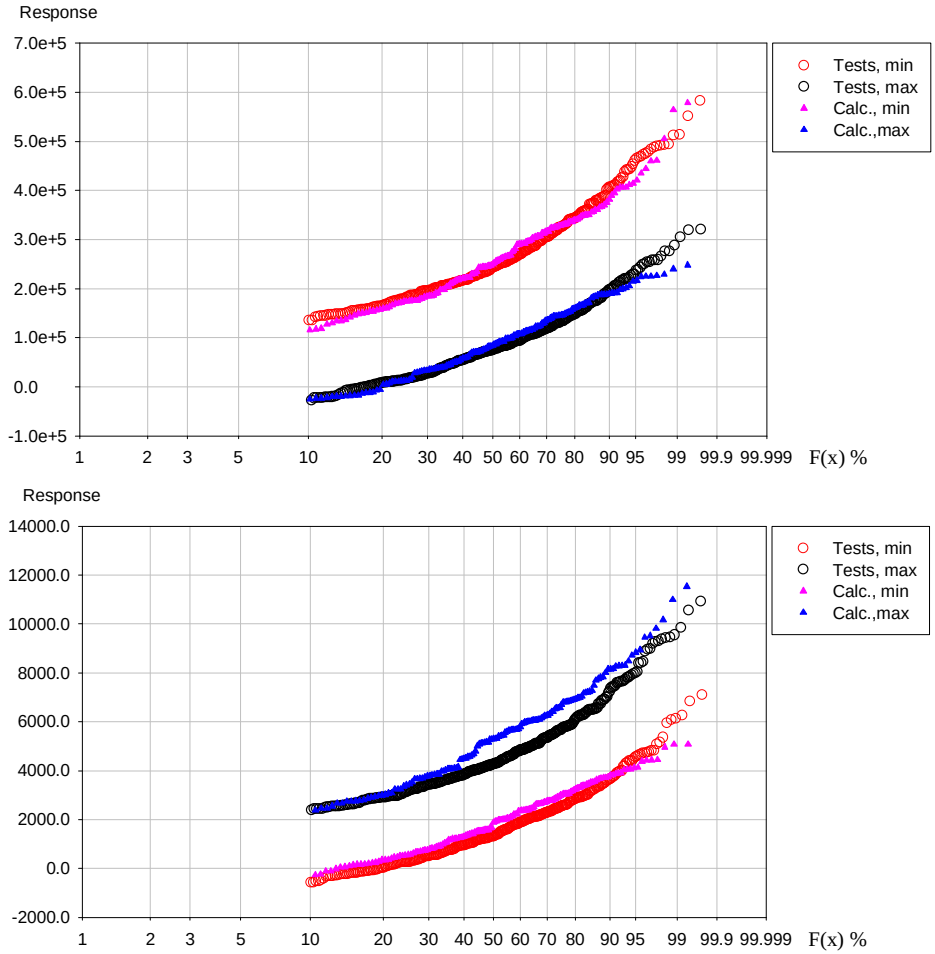

Figure 4.6. Amplitude peaks from model tests and calculations. Top: Vertical bending moment amidships (kNm). Bottom: Vertical shear force at fore ship (kN). Sea state H_s = 5.0 m and T_z = 8.5 s in head seas at forward speed of 19.1 knots.

Table 4.3. The most probable extreme values (MPEV) of the response amplitudes in the sea states of three hours, H_s = 9.0 m and T_z = 10.5 s, zero forward speed. The calculated and model test predictions are based on the fitted Weibull distributions.

U = 0 kn, 180° H_s = 9.0 m, T_z = 10.5 s	**Model test Maximum**	**Calculation Maximum**	**Model test Minimum**	**Calculation Minimum**
Wave (m)	9.9	9.4	–8.3	–9.3
Heave (m)	4.7	4.9	–4.6	–4.5
Pitch (deg)	8.3	10.1	–7.2	–7.3
Heave acceleration (m/s^2)	1.2	1.4	–1.1	–1.5
Bending (MNm)	456	519	–670	–804
Shear (MN)	13	18	–10	–10

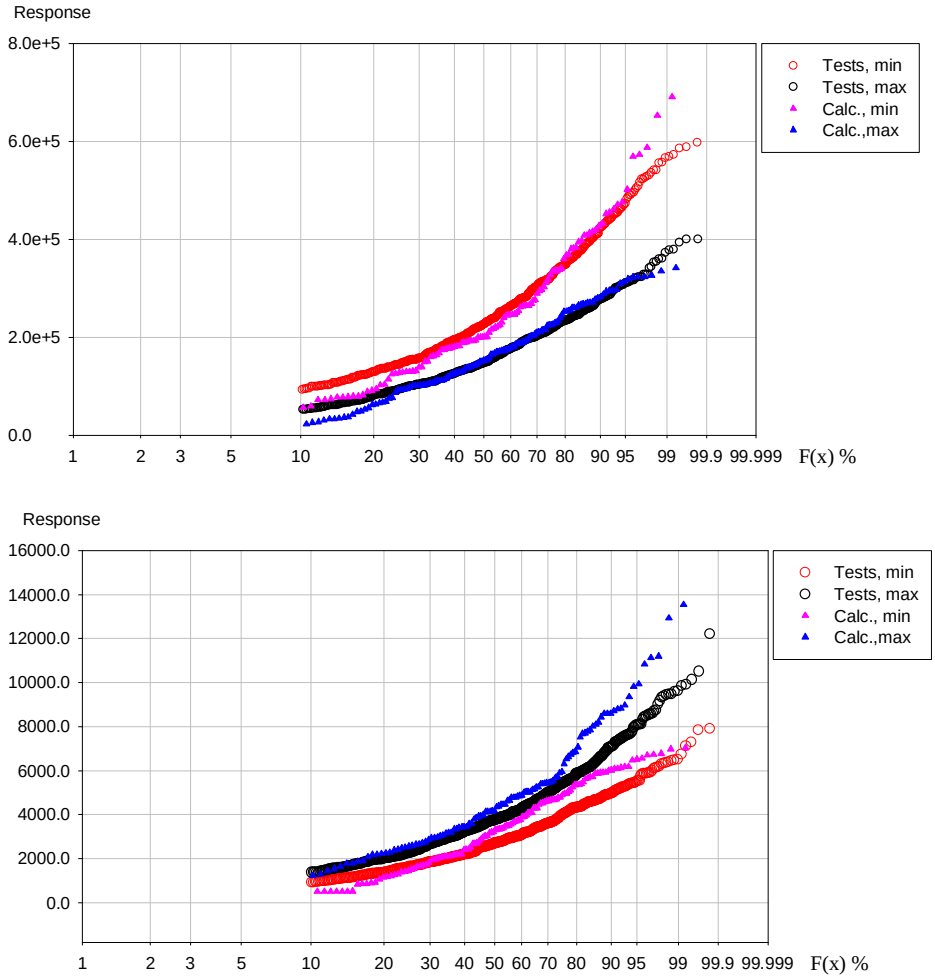

Figure 4.7. Amplitude peaks from model tests and calculations. Top: Vertical bending moment amidships (kNm). Bottom: Vertical shear force at fore ship (kN). Sea state H_s = 9.0 m and T_z = 10.5 s in head seas at zero forward speed.

5 Conclusions

The present project was focused on the hydrodynamic responses in waves and the emphasis in the investigations was on the nonlinear wave loads especially on the nonlinearities in the hull girder loads. One of the aims of the present project was to get insight of design wave loads for novel ship types and to obtain reliable numerical method for nonlinear ship-wave interaction problems to structural analyses. In addition, statistical predictions were also studied in order to estimate the extreme wave induced loads. The project consisted of numerical and experimental investigations. Model test was carried out to get insight into the important factors of nonlinear effects and to obtain validation data for the numerical simulations. Theoretical background of nonlinear effects was studied and numerical methods was developed and applied during the project.

The calculation method used in wave load predictions was based on time domain representation of the Green function. The nonlinear free surface boundary condition was linearized but the exact body boundary condition was applied on the body surface. In the body nonlinear solution all the pressure components were calculated at the instantaneous position of the ship. In addition the nonlinearity in hydrostatic and Froude-Krylov forces and moments can be included to the solution also. The nonlinear hydrostatic and Froude-Krylov forces and moments were calculated up to the actual incoming wave surface. In the calculation the most time consuming part was the solution of the time dependent Green function. In the developed computer application the Green function was solved beforehand and the results were stored in the file. In the beginning of the simulations the table of the Green function terms was read into the computer's memory. During the simulation the Green function values were interpolated from the matrix using finite element shape functions. The pre-calculated values were modelled as global finite element mesh. During the simulation the nodal values for interpolation can be easily found from the global element mesh. One advantage of the numerical integration approach was that the same solution strategy can be applied in the whole solution domain without splitting the domain in different subdomain. The method using pre-calculated Green function terms was significantly faster than the solution of Green function terms at each time step.

Validation and verification of the developed calculation method were given for the hemisphere and the Wigley hull form. The added mass and damping coefficients were calculated for the hemisphere and the results were compared to the analytical solutions. The calculated impulse response functions and the added mass and damping coefficients correlated well with analytical solution. For Wigley hull form the calculations were carried out using the body linear and nonlinear versions of the program. The calculated forces and moments corresponded well with the measured ones in spite of the rather coarse panel mesh. The heave and pitch motions were somewhat lower level than the model test results. The body linear and nonlinear versions gave the same type of the results. The calculated phases correlated well with the model test results.

Model tests were carried out for Seatech-D ship model to measure ship motions and hull girder loads in regular and irregular head waves. The calculations gave good predictions for the wave induced responses comparing to the model test results.
Responses in still water were calculated in time domain as well as measured in model tests. The aim was to investigate the steady flow effects on the bending moment and shear force

responses due to the pressure variation and the wave elevation. The shear forces and bending moments were increasing when the speed increased. The forward speed effects induced sagging bending on the hull girder. The correlation between calculations and model tests was good.

The calculated results in regular waves at zero and forward speed gave good results for the ship motions comparing to the model test results. The difference between sagging and hogging bending moments as well as in the vertical shear forces could be distinguished well. The shear forces and bending moments were well predicted by the nonlinear time domain calculations but differences existed at zero speed.

The forward speed effect due the sinkage of the ship can be seen in heave response and in vertical bending moments and shear forces. The difference in sagging and hogging can be partly explained by the steady flow effects due to forward speed. The steady bending moment in sagging was the major contribution at the lower wave amplitude but had quite small effects at higher waves. Furthermore the nonlinear effects in shear forces were also clear and difference existed in sagging and hogging conditions. The nonlinearities in shear forces are not usually considered in wave load analyses.

The nonlinear effects in the hull girder loads can be explained with the body geometry and changes in above and below the mean water level. The important factor was also the loads at the bow and stern of the ship. The given maximum and minimum amplitude peaks from regular wave tests and calculations were obtained directly from the time histories. The time histories of the responses include also local peaks and valleys between the global ones. Hence the given figures with the maximum and minimum amplitudes do not give the whole picture of the behaviour of the response in regular waves.

Based on model test results in regular waves the hogging moment was well predicted at zero speed and at the forward speed. The sagging moment was well predicted at forward speed but the calculated results deviated from the model test results at zero speed. The difference can be due to the flat stern bottom close to water line. The rapid change in geometry due to the relative motions is challenging in the calculations.
The zero forward speed calculations in irregular waves were calculated also applying improved methods and using more accurate calculation parameters. The new calculations were performed using higher order integration rule instead of the midpoint rule and using smaller panel sizes at aft body. In addition the time derivative of the velocity potential was solved directly using the boundary value problem approach.
The improved calculations gave clearly better results than the original calculations. The global hull girder loads were close to the model test results. On the other hand, the calculation time was considerably longer because of the higher order integration rule. However, the calculations gave promising results and the accuracy of the calculated results was significantly improved. Systematic calculations and further investigations should be carried out to investigate the effect of the different calculation parameters as well to investigate the theoretical approaches to model the physical phenomena correctly.

The impact at the flat stern bottom has large influence on the sagging loads in the calculated results but based on the model tests the effect was overestimated in the calculations. At higher forward speeds the bow submergence and bow impact have obviously larger effect on the global hull girder loads than the zero speed stern impacts. However, in the present method the numerical solution for impact type loads is not properly taken into account and the effects due to rapid changes in hull geometry at flat stern bottom should be further studied.

The extreme value predictions from the calculations correlate well with the model test results. The calculation method can predict the important responses that are needed in the structural

analyses. The calculations and extreme value predictions were carried out and the analyses showed that the method can be applied in demanding structural analyses. However, the calculation time is still too long that the nonlinear time domain method can be apply several different operating and environmental conditions. Linear frequency domain methods are still important to define the design sea states for different responses and hydrodynamic analyses.

References

Baarholm, G. S. and Moan, T. (2001). Application of Contour Line Method to Estimate Extreme Ship Hull Loads Considering Operational Restrictions. *Journal of Ship Research* **45:3**, 228–240.

Beck, R. and Reed, A. (2000). Modern seakeeping computations for ships. *Proc. 23rd Symposium on Naval Hydrodynamics*, Office of Naval Research ONR, 43 p.

Bingham, H.B., Korsmeyer, F.T., Newman, J.N. and Osborne, G.E. (1994). The simulation of ship motions. *6th International Conference on Numerical Ship Hydrodynamics*, 561-579.

Chang, M. (1977). Computations of three-dimensional ship motions with forward speed. *The Proc. Second Int. Conf. on Numerical Ship Hydrodynamics*, 124-135.

Chuang, J. M., Qiu, W. and Peng, H. (2007). On the evaluation of time-domain Green function. *Ocean Engineering* **34**, 962-969.

Clement, A. H. (1998). An ordinary differential equation for the Green function of time-domain free-surface hydrodynamics. *Journal of Engineering Mathematics* **33**, 291-217.

DNV. (2005). *Fatigue assessment of ship structures*. Det Norske Veritas, DNV Classification Notes No. 30.7.

Ferrant, P. (1991). A coupled time and frequency approach for nonlinear radiation. *18th Symposium on Naval Hydrodynamics*, 67-83.

Greco, M. (2001). *A Two-dimensional Study of Green-Water Loading*. Doctor Thesis. Department of Marine Hydrodynamics Faculty of Marine Technology, Norwegian University of Science and Technology, Trondheim, Norway.

Guedes Soares, C., Bondini, F., Brown, D.T., Cariou, A., Engle, A., Kuroiwa, T., Mavrakos, S., Nedergaard, H., Nielsen, F.G., Schellin, T.E. and Tan, P.S.G. (2000). Technical Committee I.2 Loads. *14th International Ship and Offshore Structures Congress (ISSC)*, Nagasaki, Japan.

GWS. (1986). *Global wave statistics*. Edited by Hogben N., Dacunha N. M. C. & Olliver G. F., British Maritime Technology Limited (BMT). Published by Unwin Brothers Limited. 661 p. ISBN 0 946653 38 0.

Hulme, A. (1982). The wave forces acting on a floating hemisphere undergoing forced periodic oscillations. *Journal of Fluid Mechanics* **121**, 443-463.

IACS. (2001). *Standard wave data*. IACS Recommendation No. 34, 2001.

Inglis, R. B. and Price, W. G. 1982. A three dimensional ship motion theory: Calculation of wave loading and response with forward speed. *Trans. RINA* **124**, 141-157.

Iwashita, H. and Ohkusu, M. (1989). Hydrodynamic forces on ship moving with forward speed in waves. *Journal of Society of Naval Architects of Japan* **166**.

Iwashita, H. (1997). Numerical seakeeping calculations based on the 3-D Green function method. *Ship Technology Research* **44**, 111-132.

Journee, J. M. J. (1992). Experiments and Calculations on four Wigley Hullforms. TU Delft, MEMT 21.

Kukkanen T. and Mikkola T. P. J. (2004). Fatigue assessment by spectral approach for the ISSC comparative study of the hatch cover bearing pad. *Marine Structures* **17**, 75-90.

Lin, W.-M. and Yue, D. (1991). Numerical solution for large-amplitude ship motions in the time domain. *18th Symposium on Naval Hydrodynamics*, 41-66.

Mäkinen, H. (2005). *Global and local FE models in the fatigue analysis of ships*. Master's thesis. Helsinki University of Technology, Department of Mechanical Engineering, Espoo, Finland (in Finnish)

Newman, J. N. (1978). The theory of ship motions. *Advances in Applied Mechanics* **18**, 221-283.

Newman, J. N. (1992). Approximation of free-surface Green functions. *Wave Asymptotics*. Cambridge Univeristy Press, 107-135.

Sen, D. (2002). Time-domain computation of large amplitude 3D ship motions with forward speed. *Ocean Engineering* **29**, 973-1002.

Wang, L. and Moan, T. (2004). Probabilistic analysis of nonlinear wave loads on ships using Weibull, Generalized Gamma, and Pareto distributions. *Journal of Ship Research* **48:3**, 202-217.

Wehausen, J. V. and Laitone, E. V. (1960). *Surface waves*. Encyclopedia of Physics, Volume IX, Fluid Dynamics III. Springer-Verlag. 446-778.

Wu, G. X. (1998). Hydrodynamic force on a rigid body during impact with liquid. *Journal of Fluids and Structures* **12**, 549-559.